



## ABSTRACT

10 The relationship between gravity wave momentum fluxes and local wind  
11 speed is investigated using probability [density](#) functions conditional on the  
12 wind speed. The motivation is to identify relationships between gravity waves  
13 and diagnostics of the large-scale flow, in order to describe synthetically the  
14 gravity wave field and provide constraints for the modeling of these waves.  
15 Three independent datasets covering high latitudes in the Southern Hemi-  
16 sphere springtime are analyzed: simulations with a mesoscale model, analyses  
17 from the European Center for Medium-Range Weather Forecasts and obser-  
18 vations from superpressure balloons of the Concordiasi campaign in 2010. A  
19 remarkably robust relation is found, with stronger momentum fluxes much  
20 more likely in regions of strong winds. The tails of the probability [density](#)  
21 functions are well described as lognormal. The median momentum flux in-  
22 creases linearly with background wind speed: for winds larger than  $50 \text{ m s}^{-1}$ ,  
23 the median gravity wave momentum fluxes are about 4 times larger than for  
24 winds weaker than  $10 \text{ m s}^{-1}$ . From model output, this relation is found to be  
25 relevant from the tropopause to the mid-stratosphere at least, and to increase  
26 somewhat with height. It is argued that two major processes that contribute  
27 to this relation are the location of tropospheric sources near the upper-level  
28 jet, and the lateral propagation into regions of strong winds. The absence of  
29 this latter effect in most gravity wave parameterizations likely will make it  
30 difficult for parameterizations to account for this relation in the stratosphere.

## 31 **1. Introduction**

32 Internal gravity waves constitute a ubiquitous component of atmospheric motions, with horizon-  
33 tal scales ranging from a few kilometers to more than a thousand kilometers (Fritts and Alexander  
34 2003). These scales imply that at least **some** of their impacts **need** to be represented by parameter-  
35 izations in atmospheric circulation models (Kim et al. 2003). They also imply that comprehensive  
36 measurements of atmospheric gravity waves constitute a tremendous challenge (Alexander et al.  
37 2010): global observations (from satellites) do not have a fine enough resolution to describe the  
38 whole spectrum, and measurements with a finer resolution generally provide only a limited spa-  
39 tial coverage. Progress is expected to come from collaborative efforts combining observations and  
40 high-resolution modelling, as illustrated by the recent comparisons between observed and modeled  
41 gravity waves (Geller et al. 2013).

42 One of the most significant impacts of gravity waves results from the dynamical forcings they  
43 produce in the middle atmosphere (Andrews et al. 1987; Fritts and Alexander 2003): their dissi-  
44 pation induces a convergence of the momentum fluxes (MF) they transport and hence a dynamical  
45 forcing. Many studies have focused on quantifying momentum fluxes and describing their geo-  
46 graphical and seasonal variations (e.g. Alexander et al. (2008); Ern et al. (2011)), to be compared  
47 with their modeled counterparts, parameterized or resolved.

48 Over the last decade, considerable progress has been made on the observations of the GWs in  
49 the lower stratosphere and the middle atmosphere. This progress follows the considerable im-  
50 provements in satellite measurements (e.g. Ern et al. (2004)) and in their use and interpretation  
51 (Alexander 2015), but also from in-situ balloons observations (Vincent et al. 2007; Geller and Gong  
52 2010). These observations, coupled to high resolution simulations reveal that the GW field is more  
53 intermittent than anticipated (Hertzog et al. 2008; Alexander et al. 2010), questioning the way

54 GWs are currently parameterized: having a few intense wave episodes rather than a continuous  
55 source with small intensity changes completely the altitudes at which the waves may be expected  
56 to dissipate and force the background flow. The [intermittency in time and space of the parame-](#)  
57 [terized gravity waves can be improved](#) by parameterizations that relate the gravity waves to their  
58 tropospheric sources. Whereas this is now commonly done for convective gravity waves (using  
59 schemes like Beres et al. (2004); Song and Chun (2005); Lott and Guez (2013)), this is rather  
60 the exception for non-orographic gravity waves parameterizations (Charron and Manzini 2002;  
61 Richter et al. 2010). The recent stochastic parameterization of de la Camara and Lott (2015) stands  
62 out as having been adapted to incorporate and reproduce this intermittency with a physically based  
63 link to the tropospheric flow (Lott et al. 2010, 2012). Nonetheless, there is a pressing need for en-  
64 hanced understanding of non-orographic gravity waves and improved parameterizations of these  
65 waves (Kim et al. 2003; Plougonven and Zhang 2014). One would wish for a quantitative relation  
66 between the large scale flow and the characteristics of gravity waves that are found near jets and  
67 fronts. The gravity wave field near realistic jets and fronts is however complex (e.g. Zhang et al.  
68 (2001); Waite and Snyder (2012); Plougonven et al. (2015)), and it is perhaps more reasonable not  
69 to aim for a deterministic relation between the large scale flow and gravity wave characteristics,  
70 but rather identify factors in the large scale flow that most efficiently constrain the waves likely to  
71 be found at a given time and location.

72 The probability [density](#) function (PDF) of absolute momentum fluxes provides a good means to  
73 quantify intermittency and to compare different sources of information on gravity waves (Hertzog  
74 et al. 2012), and it is now also used to analyze gravity waves in satellite data (Wright et al. 2013).  
75 This intermittency was also explored in outputs of numerical models (Plougonven et al. 2013;  
76 Jewtoukoff et al. 2015). Comparison of modeled gravity [waves](#) in analyses from the European  
77 Center for Medium-range Weather Forecasts (ECMWF) waves to observed gravity waves have

78 shown very encouraging agreement (Plougonven and Teitelbaum 2003; Wu and Eckermann 2008;  
79 Shutts and Vosper 2011; Plougonven et al. 2013; Jewtoukoff et al. 2015). Relative to observations,  
80 modelled gravity wave fields offer the advantage of providing a more extensive dataset to test and  
81 explore factors that may be crucial in shaping the gravity wave field.

82 Now, over the Southern polar cap, mesoscale simulations also tell that, on top of the sources,  
83 the dynamical filtering of the gravity waves by the background flow is also essential to interpret  
84 their regional and vertical distributions: more precisely, maps of mean gravity-wave MF suggest  
85 that larger values are found in regions corresponding to the mean position of the stratospheric jet  
86 (e.g. Sato et al. (2012)), and examination of snapshots of the flow above the Southern Ocean (e.g.  
87 Figure 1) suggests that, also in instantaneous distributions, strong values of momentum fluxes  
88 are more likely to occur in the stratospheric jet than outside of it. Regions of strong winds (i.e.  
89 the polar vortex) have been highlighted for a long time as a favored locus for gravity waves, for  
90 reasons that are at least partly tied to lateral propagation (Dunkerton 1984; Whiteway et al. 1997;  
91 Sato et al. 2009).

92 The aim of the present study is to [describe and quantify](#) the relation between non-orographic  
93 gravity waves and the strength of background stratospheric wind. The tool used will be the PDFs  
94 of the absolute gravity wave momentum flux (GWMF), and the region and season of interest is  
95 the Southern polar cap during austral spring. This choice results from the availability of relevant  
96 and complementary datasets (see below), but is also motivated by recent studies on the belt of  
97 enhanced gravity wave activity observed in the lower stratosphere in austral winter (Hendricks  
98 et al. 2014). This belt may be connected to the difficulty of models to describe the breakdown of  
99 the polar vortex in spring: it is suspected that this bias comes in part from missing gravity wave  
100 drag (McLandress et al. 2012; de la Camara et al. 2016).

101 The datasets used include mesoscale simulations (Plougonven et al. 2013) and observations col-  
102 lected on superpressure balloon during the Concordiasi campaign (Rabier and coauthors 2010).  
103 The simulations have the advantage of providing a wide spatial and temporal coverage. The bal-  
104 loon observations used constitute the most recent and accurate dataset available for gravity waves  
105 above the Southern polar cap (Geller et al. 2013).

106 The paper is organized as follows. Section 2 introduces the data used and methodology. The  
107 relation between gravity wave momentum fluxes and the local wind speed is explored in section 3,  
108 using PDF conditional on the background wind speed. The processes that may be contributing to  
109 this relation are discussed in section 4. Implications, limitations and perspectives are discussed in  
110 section 5.

## 111 **2. Data and methodology**

112 Several datasets are used in order to explore the relation of GWMF to background wind speed:

- 113 • mesoscale numerical simulations over the Southern polar cap, run for two months in the  
114 Austral spring of 2005 with a resolution of  $dx = 20$  km;
- 115 • analyses of the European Center for Medium-Range Weather Forecasts (ECMWF), for the  
116 months of September 2010 to January 2011, corresponding to the Concordiasi campaign.  
117 The resolution of the model was T1279, corresponding to a horizontal resolution of  $0.125^\circ$  or  
118 about 13 km, with 91 vertical levels corresponding approximately to 500m vertical spacing.
- 119 • superpressure balloon measurements from the Concordiasi campaign, with the gravity waves  
120 analyzed using wavelets and taking advantage of the quasi-Lagrangian behavior of the bal-  
121 loons (Hertzog et al. 2008; Vincent and Hertzog 2014).

122 The resolution and limitations of each dataset are summarized in table 1. In the mesoscale sim-  
123 ulations, no gravity wave parameterization is used. In the ECMWF analyses, only the resolved  
124 waves are investigated. In the three datasets, in order to investigate only non-orographic gravity  
125 waves, we analyze the gravity wave MF over the oceans and far from islands or coastline (region  
126 5 of Plougonven et al. (2013)).

127 The numerical dataset is derived from mesoscale simulations carried out with the Weather Re-  
128 search and Forecast Model (WRF, Skamarock et al. (2008)), with a domain encompassing Antarc-  
129 tica and the Southern Ocean and for a time period of two months from October 21st to December  
130 18th, 2005. The domain covers an area  $10,000 \times 10,000$  km wide centered on the South Pole, with  
131 a resolution of  $dx = 20$  km in the horizontal and 120 levels going up to 5 hPa, see Plougonven  
132 et al. (2013) for a complete description. Comparison with balloon observations from the Vor-  
133 core campaign (Hertzog et al. 2008) showed good agreement between the simulated and observed  
134 momentum fluxes (Plougonven et al. 2013; Hertzog et al. 2012), though both suffered from under-  
135 estimation because of the limited resolutions.

136 The balloon measurements used come from the Concordiasi campaign which took place in the  
137 austral spring of 2010 (Rabier and coauthors 2010). Long-duration balloons provide one of the  
138 most accurate estimates of GWMF (Geller et al. 2013). The temporal resolution of measurements  
139 for Concordiasi has been greatly enhanced relative to previous campaigns (measurements every  
140 30s instead of every 15 min), allowing to resolve the full spectrum of gravity waves, hence our  
141 choice of this campaign rather than Vorcore. In the balloon observations, the momentum fluxes  
142 are estimated with a wavelet analysis of the timeseries of velocity and pressure (see Hertzog et al.  
143 (2008) and Vincent and Hertzog (2014) for details).

144 These datasets have been inter-compared previously: the mesoscale simulations have been vali-  
145 dated with data from the Vorcore superpressure campaign (Hertzog et al. 2008; Plougonven et al.

146 2013; Hertzog et al. 2012), and the ECMWF analyses have been shown to contain realistic gravity  
147 waves by comparison to the Concordiasi campaign Jewtoukoff et al. (2015). [The reader is directed](#)  
148 [to these earlier studies for an intercomparison of these datasets.](#)

149 The gravity wave field is characterized by the PDF of the absolute momentum fluxes,  
150  $\rho \sqrt{(u' w')^2 + (v' w')^2}$ . In the model output, the momentum fluxes are obtained by high-pass filter-  
151 ing spatially the velocity components, see Plougonven et al. (2013) and Jewtoukoff et al. (2015) for  
152 further details. The observed momentum fluxes are obtained after a wavelet-based identification  
153 of wave packets in the time series of velocity (Boccaro et al. 2008; Vincent and Hertzog 2014).

### 154 **3. Relation between gravity waves and local wind speed**

155 In order to investigate only non-orographic gravity waves, we analyze the gravity wave MF over  
156 the oceans (region 5 of Plougonven et al. (2013)). In order to compare with superpressure balloons,  
157 the analysis of model output is carried out at  $z = 20$  km. This is slightly higher than the flight  
158 levels of the balloons (between 17 and 19 km).

#### 159 *a. In different datasets*

160 Gravity wave momentum fluxes in the mesoscale simulations documented by Plougonven et al.  
161 (2013) [are](#) first investigated. PDFs of absolute momentum fluxes were obtained, [using 200 bins](#)  
162 [that are equally spaced for the logarithm of the GWMF.](#) The PDFs are conditional on the back-  
163 ground windspeed  $U(x, y, z, t)$  [\(i.e. simply the total wind speed at that location and time\)](#) which  
164 was partitionned in intervals of  $10 \text{ m s}^{-1}$ , see Figure 4: [for example the green curve corresponds to](#)  
165  [\$p\(F | 30 < U < 40 \text{ m s}^{-1}\)\$ , i.e. the probability to find the value F of the GWMF, knowing that the](#)  
166 [background wind is between 30 and 40  \$\text{m s}^{-1}\$ .](#) Each of these curves, by definition, is normalized  
167 [such that  \$\int\_0^\infty p\(F | 30 < U < 40 \text{ m s}^{-1}\) dF = 1\$ .](#) Finally, note that the vertical axis is logarithmic,



168 to provide detail on the tail of the distributions (rare but intense events which account for a large  
169 part of the average GWMF (Hertzog et al. 2012)). Strikingly, the PDFs are found to be very con-  
170 strained by the background wind, with the frequency of occurrence of GWMF larger than 5 mPa  
171 systematically increasing with background horizontal wind speed  $U$ . For example, values of the  
172 GWMF between 35 and 40 mPa are about 100 more likely where the wind is larger than  $50\text{m s}^{-1}$   
173 than where the wind is weaker than  $10\text{m s}^{-1}$ . Note finally that the graphs (semilog in the vertical  
174 axis) purposefully emphasize the tails of the PDFs: because of the intermittency of the gravity  
175 waves, it is the rare, large events described by the tail of the PDF that matter most (Hertzog et al.  
176 2012). The thin lines in Figure 4 are lognormal approximations of the PDFs, to be discussed in  
177 the following subsection.

178 Figure 5 shows the PDFs of GWMF estimated from the ECMWF analyses, over the same ge-  
179 ographical region but for the time of the Concordiasi campaign. Again, strikingly, the PDFs of  
180 momentum fluxes are stratified by the background velocity. The values of the momentum fluxes  
181 are somewhat larger than those found in the WRF simulations, by a factor 2-3. This is consistent  
182 with the expected sensitivity to resolution, whether based on sensitivity tests (Plougonven et al.  
183 2013) or on the truncation of the spectrum of resolved waves (Jewtoukoff et al. 2015).

184 Figure 6 shows the PDFs of GWMF in balloon observations, conditional on the background wind  
185 speed. Relative to Figures 4 and 5, there are surprising similarities and expected differences. The  
186 differences include the more irregular nature of the PDFs, expected from a more limited sampling,  
187 and the significantly larger values of the GWMF, expected because of the limited resolution of the  
188 simulations, see discussion in Jewtoukoff et al. (2015). It is worth stressing that these curves are  
189 obtained from *in situ* measurements, and that most of the information is in the tail of the PDFs, i.e.  
190 carried by few, rare events. Hence, it is normal that the curves are noisier than the ones obtained  
191 from model output. The ordering of the PDFs is not as perfect as for model output. Nonetheless,

192 the overall picture is again that the tails of the PDFs are generally ordered by the background  
193 windspeed, with small exceptions that are compatible with noise due to the limited sampling.  
194 Hence the main result we retain is the similarity and confirmation of a strong sensitivity of the  
195 PDF to the windspeed. Again, for GWMF values larger than 10 mPa, the curves are generally  
196 ordered according to the background wind speed, and the occurrence frequency of large GWMF  
197 varies by more than one order of magnitude as a function of  $U$ .

198 In summary, information on the local wind speed in the lower stratosphere already provides  
199 significant information about the GWMF that are likely present. This has been obtained over the  
200 ocean for the Southern high latitudes in austral spring. The preference for strong GWMF values  
201 to be present in regions of strong windspeeds comes out with striking agreement from the three  
202 datasets, whether from observations or from models, and therefore we consider this a very robust  
203 result. It is consistent with a well-known aspect of the spatial distribution of GWMF, i.e. the belt  
204 of large values found in the stratospheric polar vortex (Hendricks et al. 2014). This belt has been  
205 noted in a number of previous studies in time-averaged fields, not from instantaneous values. It  
206 has been argued that horizontal propagation and refraction into the jet contributed to this spatial  
207 distribution of the gravity waves (Dunkerton 1984; Sato et al. 2009). The present approach sheds  
208 a different light on this phenomenology: without reference to geography, it may provide a useful  
209 and compact quantification of this preference for large GWMF to be present in regions of strong  
210 winds.

211 Figure 7 shows the medians and the geometric standard deviations in the three datasets, as a  
212 function of the background wind speed  $U$ . The medians have been normalized for the compari-  
213 son, whereas the geometric standard deviations naturally are dimensionless (Limpert et al. 2001).  
214 Both the values directly calculated from the series of GWMF values (left column) and the values  
215 describing the lognormal fits (right column) are displayed. The main, robust conclusion to retain

216 from these panels is that the medians systematically increase with the background wind speed, the  
217 increase being surprisingly consistent between the different datasets (factor 3 to 5 between the me-  
218 dian for the weakest winds and for the strongest winds). The geometric standard deviations vary  
219 significantly from one dataset to another (with the observations in between the two values from  
220 the models), but within a dataset they are remarkably insensitive to the background wind speed.

## 221 **4. Interpretation**

222 The relation highlighted in the previous section appears remarkable because it is robust across  
223 several datasets, and because it is simple and can be very succinctly summarized (section 3A1  
224 above). In the present section, we try and identify processes that may contribute to this relation,  
225 and then further explore this relation in model output and with an offline parameterization, dis-  
226 cussing implications for the relevance of the different candidate processes.

### 227 *a. Candidate processes*

228 Several processes are likely to play a role and contribute to the relation between GWMF and  
229 background wind speed:

- 230 1. [alignment in the vertical of the tropospheric sources and of strong stratospheric winds above:](#)  
231 the distribution of sources below may have its maxima coinciding with the polar vortex, with  
232 vertical propagation sufficient to yield more intense GWMF in regions of strong winds.
- 233 2. Wind filtering: critical levels remove waves with phase velocities matching the wind (An-  
234 drews et al. 1987). Regions of strong stratospheric winds may correspond to locations below  
235 which there has been less filtering, the strong winds allowing more of the gravity wave spec-  
236 trum to go through.

- 237 3. Lateral propagation of waves: lateral propagation and focusing into the jet is known to occur  
238 (Dunkerton 1984; Sato et al. 2009, 2012), and can lead to enhanced GWMF in regions of  
239 strong winds.
- 240 4. shear as a source of waves: a strong wind speed in the lower stratosphere may oftentimes be  
241 associated with strong shear between the troposphere and the stratosphere. Now PV anoma-  
242 lies in shear may act as a source of gravity waves (Lott et al. 2010, 2012).

243 The different processes outlined above are expected to have different signatures on the relation  
244 between GWMF and local windspeed. In the following sections we explore the relation between  
245 GWMF and wind speed further, and use those results to discuss the possible relevance of the  
246 mechanisms 1-4 outlined above.

#### 247 *b. Variation with altitude*

248 The output of the WRF simulations and of the ECMWF analyses document the relation of  
249 GWMF and wind speed at different heights. Figure 8 shows the PDFs of GWMF conditional  
250 on the background wind for several heights from the tropopause to the mid-stratosphere. Strik-  
251 ingly, the sensitivity of the PDFs holds at these different altitudes. As expected from previous  
252 investigations (e.g. Hertzog et al. (2012)) momentum fluxes decrease with height, and the tails  
253 of the PDFs diminish significantly with height. Similar figures were obtained from the ECMWF  
254 analyses, at heights of 10, 15, 20 and 30 km. Again, the figures (not shown) are characterized  
255 by a robust relation between momentum fluxes and background wind speed at all heights, and the  
256 expected decrease of momentum fluxes with height.

257 In order to determine how the sensitivity of momentum fluxes evolve with height, figure 9 sum-  
258 marizes the variations with background wind speed of the median momentum fluxes, for the dif-

259 ferent heights and for the two different models. Again, the medians are normalized by the mean  
260 of the medians for  $20 < U < 30 \text{ ms}^{-1}$  and  $30 < U < 40 \text{ ms}^{-1}$ . The two figures are remarkably  
261 similar, showing first that the relation is robust and holds at different heights, second that the slope  
262 increases a little with height, and third that it deviates from a linear relation at the lowest and  
263 highest heights.

264 Assuming that the sources for momentum fluxes are in the troposphere, the sensitivity of the  
265 GWMF PDF to the background wind bears different meanings at different heights: in the low-  
266 ermost stratosphere, this suggests that the sources are tied to the jet region, which is expected  
267 (Plougonven and Zhang 2014). Higher in the stratosphere, and given that larger momentum fluxes  
268 in the upper-troposphere are associated with strong winds, it shows that the propagation does not  
269 counteract this relation, and in fact somewhat enhances it. Lateral propagation into the regions of  
270 stronger winds and critical filtering in regions of weak winds both will tend to enhance the sensi-  
271 tivity of GWMF to  $U$ . The present analysis does not allow to conclude on the relative importance  
272 of both effects.

273 If strong stratospheric winds were simply co-located in the vertical with strong upper-  
274 tropospheric winds, the PDFs of momentum fluxes in the stratosphere should have the same sen-  
275 sitivity to tropospheric winds as to local wind. Figure 10 illustrates that this is not the case by  
276 displaying PDFs of GWMF at 30 km altitude, conditional on the wind speed at 10 km. Although  
277 there is still some sensitivity, most of the information has been lost and the different PDFs are  
278 no longer sorted by knowledge of the wind speed below. This constitutes some evidence for the  
279 importance of lateral propagation that has already been emphasized by other means in previous  
280 studies (Sato et al. 2012; Senf and Achatz 2011; Ribstein et al. 2015).

281 Another piece of evidence for lateral propagation comes from the PDF of the orientation of the  
282 wave momentum flux relative to the background wind at  $z = 20 \text{ km}$ , shown in figure 11. This

283 was calculated from the WRF simulations by calculating the angle, at all locations over the ocean,  
284 between the momentum flux vector and the local wind. As seen from figure 3, both the north and  
285 south sides of the jet core are sampled in the oceanic region used for the present analysis. Waves  
286 are predominantly found to propagate against the flow, i.e. angles between 90 and 270 degrees.  
287 Moreover, there is a strong asymmetry with the mode of the PDF corresponding to an angle of  
288 about 225 degrees. Knowing that the winds in the polar vortex are predominantly westerlies, this  
289 is indicative of poleward propagation, from source regions located more to the North. Finally,  
290 note that this figure is reminiscent of the PDF of the orientation of gravity wave momentum fluxes  
291 that was displayed in Plougonven et al. (2015) (their figure 21), but with a somewhat stronger  
292 anisotropy.

### 293 *c. Tropospheric sources*

294 The spatial variations of the gravity wave field is, evidently, in part tied to those of the sources.  
295 Nonetheless, this information may be more difficult to capture because non-orographic sources  
296 other than convection remain elusive (Plougonven and Zhang 2014) and difficult to quantify.  
297 Moreover, as gravity waves ascend in the stratosphere, their propagation modulates the wave field  
298 in such a way that the background wind may, on its own, convey more information than the knowl-  
299 edge only of tropospheric sources.

300 The present section aims at testing whether simple diagnostics that are tied to tropospheric  
301 jet/front systems may provide as much information, or more, regarding the gravity wave field than  
302 the local wind speed. We restrict our considerations to diagnostics that are simple and very easily  
303 available, as was the case for the local wind speed (investigating more sophisticated diagnostics  
304 such as the frontogenesis function Charron and Manzini (2002) or the residual of the nonlinear  
305 balance equation Zhang et al. (2001) is not the purpose of the present study.) We will consider

306 vorticity, at the surface or in the mid-troposphere, and surface pressure. The former is indicative of  
307 fronts, the latter will have a signature at large scales and will point out regions of active cyclogen-  
308 esis. Other diagnostics could be proposed based on past attempts to parameterize non-orographic  
309 gravity waves (Charron and Manzini (2002); Richter et al. (2010) used the frontogenesis func-  
310 tion in mid-troposphere) or on idealized and real case studies (O’Sullivan and Dunkerton (1995);  
311 Plougonven et al. (2003); Zhang (2004); Zülicke and Peters (2006, 2008) suggest indicators of  
312 imbalance such as Lagrangian Rossby numbers and the residual of the nonlinear balance equa-  
313 tion). The range of possibilities is large and its exploration is not the purpose of the present study.  
314 The present question is merely: for the region and season of interest, is there a potential source  
315 diagnostic, having comparable simplicity to local wind speed, that carries comparable information  
316 on GWMF?

317 Figure 12 shows PDFs of gravity wave momentum fluxes, conditional on different indicators of  
318 tropospheric activity. The curves plotted are illustrative: there is very little sensitivity of the PDFs  
319 to the underlying vorticity. Similar tests were carried out using the ECMWF analyses, with similar  
320 results. In part, this results from the small-scale character of vorticity: even for gravity waves  
321 emanating from fronts, they may not show good correlation with the underlying fronts because  
322 they propagate away horizontally from the narrow maximum of vorticity which is the signature of  
323 the front. This motivated the use of surface pressure, which has signatures on larger scales and for  
324 which we expect gravity waves to be enhanced near negative anomalies (extra-tropical cyclones  
325 and regions of enhanced precipitation). The PDFs indeed show some sensitivity to this condition  
326 on surface pressure, yet the ‘stratification’ of the PDFs based on this condition is much weaker than  
327 that obtained simply from using the wind at 10 km. Hence another attempt has consisted in using  
328 vorticity as a condition, but after having averaged it spatially. Figure 13 shows the PDFs of GWMF  
329 again, conditional on the surface vorticity (top) and mid-tropospheric vorticity (bottom) averaged

330 in boxes that are 10 degrees longitude by 5 degrees latitude. The GWMF do show significant  
331 sensitivity to the last of these diagnostics, i.e. mid-tropospheric vorticity spatially averaged. This  
332 brings support to the choice made by de la Camara and Lott (2015) to use tropospheric vorticity as  
333 the indicator for non-orographic, non-convective gravity wave sources. Their motivation for this  
334 choice came from theoretical studies of waves emitted by sheared PV anomalies (Lott et al. 2010,  
335 2012).

336 While it will be of interest to explore further the sensitivity of GWMF to different indicators  
337 of the tropospheric flow, the present investigations suffice for the following conclusions: first, the  
338 sensitivity of GWMF to the background wind speed in the lower stratosphere is remarkable and  
339 it is not straightforward to find a tropospheric diagnostic that carries more, or even comparable,  
340 information. Second, [possible candidates for such a tropospheric diagnostic include the surface  
341 pressure and the mid-tropospheric vorticity \(spatially averaged for the latter, as this is a small-scale  
342 field\).](#)

#### 343 *d. Vertical propagation and parameterizations*

344 It is known that the vertical propagation of waves in the large-scale winds is sufficient to repro-  
345 duce much of the spatial variability of the gravity wave field (Alexander 1998). As a method to  
346 test how much vertical propagation, on its own, can lead to differences in the PDFs of GWMF  
347 depending on the background wind, one can use parameterizations from an Atmospheric General  
348 Circulation Model (AGCM) run in offline mode. As the near totality of GW parameterizations,  
349 the one of LMDz makes the columnar approximation, i.e. gravity waves are assumed to propagate  
350 only vertically. Two key advantages of the LMDz parameterization for the present comparison are  
351 that it has been designed to describe fluxes that are consistent with observations regarding spectra  
352 and intermittency de la Camara et al. (2014), and it includes frontal/jet sources that are physically



353 tied to the resolved tropospheric flow in the model de la Camara and Lott (2015). Following the  
354 theoretical arguments of Lott et al. (2010, 2012), the parameterization evaluates the grid-scale  
355 vorticity and Richardson number to determine the amplitude of the GWMF emitted, and as a con-  
356 sequence represents the observed GWMF intermittency reasonably well (de la Camara and Lott  
357 2015). Therefore it becomes straightforward, with this parameterization, to produce PDFs of the  
358 GWMF conditional on the background wind speed and compare those with the ones obtained  
359 above from resolved waves. Input data for the offline runs are daily wind and temperature fields  
360 from ERA-Interim for the September 2010 - January 2011 period. Results are shown at 20 km  
361 height south of 40°S. Note that the purpose here is to test the effect of vertical propagation and  
362 critical filtering (the offline runs are used as a tool to isolate vertical propagation), not to evaluate  
363 the most recent version of the constantly evolving parameterization.

364 Figure 14 shows the PDFs of GWMF conditional on background wind speed in four config-  
365 urations. The impact of having sources that are physically tied to the tropospheric flow can be  
366 seen by comparing the left and right columns: the latter shows results of an offline run of the  
367 parameterization where the initial fluxes are set to follow a lognormal distribution, but with no in-  
368 formation from the tropospheric flow. With the phase speed spectrum that is used operationally in  
369 LMDZ (i.e. a Gaussian distribution of phase speeds centered on  $0\text{ms}^{-1}$  with a standard deviation  
370 of  $40\text{ms}^{-1}$ ) the parameterized fluxes that come from homogeneous sources show no sensitivity  
371 to the background wind speed. With the same phase speed spectrum, one can see from the top  
372 left panel that the present version of the parameterization (with sources estimated from the tropo-  
373 spheric flow) does reproduce part of the sensitivity of the GWMF to the background wind speed.  
374 This reflects the collocation of the sources and high wind regions in the upper-troposphere region,  
375 as expected from previous sections. With homogeneous sources, it is possible to obtain a sensi-  
376 tivity of GWMF to background wind speed, but this requires a drastic change in the phase speed

377 spectrum (standard deviation of  $10\text{m s}^{-1}$ ). The sensitivity to the launch level was also investigated,  
378 but had little impact. Finally, the effect of reducing the phase speeds in the parameterization with  
379 varying sources was tested (lower left panel). Here again, this reduction of the phase speeds al-  
380 lows to obtain a significant dependence of the GWMF to the background wind speed. Note that  
381 this dependence remains weaker than that found in the three datasets investigated in section 3. In  
382 other words, it appears that specifying the sources from the tropospheric flow accounts for a small  
383 part of the relation between GWMF and wind speed. It would be possible to account for a more  
384 significant part of this relation by critical filtering and vertical propagation only, but this requires  
385 a drastic reduction of the phase speed spectrum, a reduction which seems unrealistic relative to  
386 observations (e.g. Jewtoukoff et al. (2015)) and would be an obstacle for the parameterization to  
387 fulfill its role in forcing the upper-stratosphere and mesosphere circulation.

## 388 **5. Summary and conclusion**

389 The relation of non-orographic gravity waves to the background flow has been investigated for  
390 waves in the Southern high latitudes in springtime. Several recent observational and numerical  
391 studies have emphasized the importance of the intermittency of the gravity wave field (Hertzog  
392 et al. 2008; Alexander et al. 2010; Hertzog et al. 2012; Plougonven et al. 2013; Wright et al.  
393 2013) and have proposed PDFs of momentum fluxes as a description of gravity wave momentum  
394 fluxes (GWMF) which includes their intermittency. We have investigated the sensitivity of PDFs  
395 of GWMF to the local background wind speed,  $U$ , in three different and complementary datasets:  
396 mesoscale simulations (Plougonven et al. 2013), analyses from the ECMWF (Jewtoukoff et al.  
397 2015) and measurements from long-duration balloons of the Concordiasi campaign (Rabier and  
398 coauthors 2010). In order to focus on non-orographic gravity waves, only oceanic regions far from  
399 orography were considered. It was found that the background wind speed provides significant

400 information on the expected gravity wave MF [in this region](#). The PDF of MF conditional on the  
401 background wind speed,  $U$ , displayed systematically longer tails and larger means for larger  $U$   
402 (figures 4, 5 and 6). Very good agreement was found between the three very different datasets,  
403 providing strong evidence that this is a very robust feature [in this region](#).

404 The present [study](#) also allowed to investigate further the description of GWMF PDFs using the  
405 lognormal distribution. Our analysis in different datasets further confirmed that the tails of the  
406 PDF are very well approximated as lognormal (Hertzog et al. 2012). Further, this also applies to  
407 subsets of GWMF.

408 The variation of the PDFs of GWMF with respect to the local wind speed was synthesized  
409 using their medians and their geometric standard deviation (Limpert et al. 2001). As expected,  
410 the medians differ in absolute value (Geller et al. 2013; Jewtoukoff et al. 2015), but their relative  
411 variations displayed remarkable consistency between the three datasets. At an altitude of 20 km,  
412 the median momentum fluxes for winds larger than  $50 \text{ m s}^{-1}$  is about 4 times larger than those for  
413 winds weaker than  $10 \text{ m s}^{-1}$ . It is noteworthy that the observational dataset falls in between the two  
414 numerical datasets. The geometric standard deviations also differ in value between the different  
415 datasets, but they are strikingly insensitive to the background wind speed. For each dataset, they  
416 appear as a rather constant parameter for the PDFs of GWMF.

417 This bias for larger MF in regions of strong winds is consistent with previous results emphasizing  
418 a belt of strong MF in the stratospheric jet (Ern et al. 2004; Alexander et al. 2010; Sato et al. 2009).  
419 Several factors may contribute to this: spatial variations of the tropospheric sources (Hendricks  
420 et al. 2014), lateral propagation (Sato et al. 2012), local generation tied to the stratospheric winds  
421 (e.g. Sato and Yoshiki (2008)) or the vertical shear (e.g. Lott et al. (2010, 2012)). The relative  
422 importance of these different processes was investigated by analyzing the variation with height of

423 GWMF, the relation of GWMF to simple indicators of tropospheric synoptic activity, and by using  
424 an offline parameterization (de la Camara and Lott 2015).

425 The sensitivity of GWMF at an altitude of 10 km was investigated. A strong sensitivity to local  
426 wind was found here too, implying that the relation above is not purely a result of propagation  
427 in the lower stratosphere. The contrast between GWMF in strong winds relative to weak winds  
428 increases somewhat with height, indicating that propagation contributes to maintain and even en-  
429 hance this relation. Nonetheless, this relation is already present at the tropopause level. This  
430 reflects that the sources are tied to the upper-tropospheric jet, which is expected. The relevance of  
431 this relation relative to other tropospheric diagnostics was evaluated by investigating PDFs con-  
432 ditional on simple tropospheric diagnostics (surface vorticity, surface pressure, mid-tropospheric  
433 vorticity). As the vorticity field has much variability at small scales, it was averaged spatially for a  
434 fair comparison. [These test suggest that the GWMF PDFs are sensitive to the surface pressure and  
435 to mid-tropospheric vorticity anomalies below.](#) The sensitivity is at best comparable to that found  
436 for local wind. This provides additional justification to the choice of parameterization made by  
437 de la Camara and Lott (2015), but further investigation would be required to explore more efficient  
438 tropospheric diagnostics.

439 This latter parameterization (de la Camara and Lott 2015) provides an ideal tool to test the role  
440 of vertical propagation and critical level filtering in the relation between GWMF and wind speed:  
441 indeed, as the waves are launched stochastically and fairly follow a lognormal distribution, plots  
442 similar to the ones obtained from observations and high-resolution models can be produced and  
443 compared. By construction, the parameterization only takes into account vertical propagation.  
444 The sources can be tied to the tropospheric flow, or they can be made horizontally and temporally  
445 homogeneous, so as to isolate the effect of vertical propagation. These tests provide evidence that  
446 confirm that the collocation of sources and high-wind regions in the upper-troposphere accounts

447 for part of the relation between GWMF and wind speed, but only for a small part. The tests further  
448 show that it is possible to reproduce part of this relation by changing the phase speed spectrum of  
449 the waves launched, but that this requires a drastic reduction of the phase speeds (factor 4 relative  
450 to what is used successfully in the online version of the parameterization). It is therefore plausible  
451 to interpret these results as indirect evidence that variability of the sources and vertical propagation  
452 alone can not account for the relation that is found in both observations and numerical models. In  
453 other words, this is likely evidence for a missing process, presumably lateral propagation.

454 Lateral propagation is known to occur (Dunkerton 1984; Sato et al. 2012). [Now, this lateral](#)  
455 [propagation is more pronounced for low-frequency waves than for high-frequency waves \(?\), and](#)  
456 [hence one might object that our analysis relies on model output which likely has a bias towards](#)  
457 [low frequencies for gravity waves ?](#). However, the presence of the relation between GWMF  
458 and wind speed in observations from Concordiasi balloons imply that this relation does not apply  
459 only to low-frequency waves: whereas the model output (WRF and ECMWF) presumably have  
460 a bias towards low-frequency waves because of their limited horizontal resolution, the balloon  
461 measurements describe the full spectrum of gravity waves (Jewtoukoff et al. 2015).

462 [Further evidence for lateral propagation stemmed from the investigation of the](#) orientation of the  
463 gravity wave momentum fluxes relative to the local wind: the most likely orientation corresponds  
464 to waves propagating against the wind but obliquely (coming from low latitudes and propagating  
465 toward the pole). This is consistent with the main source of waves being in the tropospheric storm  
466 tracks, which are more equatorward than the polar night jet, and confirms the lateral propagation  
467 already highlighted in the literature (Sato et al. 2009).

468 The purpose of the present study was to investigate the relation of GWMF to diagnostics of the  
469 large-scale flow, in the lower-stratosphere. A remarkably robust and simple relation was found  
470 between background wind speed and GWMF. It seems attractive because of its compactness and

471 robustness. This relation provides a novel and compact description of the bias for stronger GWMF  
472 in regions of strong winds. We expect such relations between gravity waves and background flow  
473 to become a tool to analyze gravity waves, test and improve parameterizations, and constitute a  
474 complement to using only geographical and seasonal variations.

475 *Acknowledgments.* The authors acknowledge support from the ANR project StraDyVariUS  
476 (Stratospheric Dynamic and Variability, ANR-13-BS06-0011-01). The WRF simulations were  
477 performed using HPC resources from GENCI-IDRIS under grants 2012-012039 and 2013-012039.  
478 AH and FL benefitted from the SPARC Gravity Wave activity and from ISSI which provided  
479 opportunities for exchanges and discussions on these topics. Concordiasi was built by an inter-  
480 national scientific group and was supported by the following agencies: Météo-France, CNES,  
481 IPEV, PNRA, CNRS/INSU, NSF, UCAR, University of Wyoming, Purdue University, University  
482 of Colorado, and ECMWF. AdIC acknowledges support from EMBRACE, and RP is thankful to  
483 N. Belabas for useful suggestions.

## 484 APPENDIX

### 485 **A1. Lognormal approximation of the tails**

486 ♠ As mentioned in section A1, the lognormal distribution may here reflect the exponential  
487 dependence of spontaneous emission on the local Rossby number (Vanneste 2013). ♠

488 The description of the PDF of momentum fluxes [highlights](#) the significant weight of rare but  
489 intense events. This emphasizes that describing sources of non-orographic gravity waves in pa-  
490 rameterizations using a constant value is probably inappropriate (de la Camara et al. 2014). Now,  
491 PDFs of GWMF could well be described by a lognormal distribution (Hertzog et al. 2012). A  
492 lognormal distribution is found for a strictly positive variable whose logarithm is normally dis-

493 tributed (e.g. Limpert et al. (2001)). Because the propagation through successive layers of the  
494 atmosphere can be seen as a succession of multiplicative reductions of the momentum fluxes, it  
495 has been argued that propagation alone could explain the relevance of lognormal distributions  
496 (Hertzog et al. 2012). But other reasons, linked to wave sources in the troposphere, may also  
497 be relevant. For example, it has been repeatedly highlighted that waves spontaneously generated  
498 are exponentially small in Rossby number (Vanneste and Yavneh 2004; Plougonven et al. 2005;  
499 Vanneste and Yavneh 2007; Lott et al. 2010). If the distribution of local Rossby number **can be**  
500 **roughly described as a Gaussian**, the spontaneously emitted waves naturally follow a lognormal  
501 distribution (Vanneste, personal communication).

502 The focus on the tails of the distribution and their presentation in semilog plots may hide the  
503 fact that the vast majority of values are very weak. To illustrate this and clarify how the PDFs  
504 are approximated with a lognormal distribution, an example is shown in Figure 15 for momentum  
505 fluxes from the WRF simulations over the ocean: the top panel shows a standard plot, emphasizing  
506 that the most likely values are close to zero, whereas the bottom panel shows a semilog plot,  
507 revealing a shallow tail which extends to large values. Two approximate distributions are overlaid:  
508 the lognormal with the same median and multiplicative standard deviation, and a lognormal that  
509 has been adjusted to better describe the tail. The adjustment is carried out using a least squares fit  
510 on the logarithms of the distribution, starting from the first percentile. Indeed, the distribution for  
511 the weakest flux values are likely less reliable than the rest of the PDF. In particular in the balloon  
512 dataset, waves are identified as wavepackets with wavelets, and there is a threshold (defined in  
513 relation to measurement uncertainties) below which waves are not detected. Including the weakest  
514 values in the fit led to erroneous results, whereas there was very little sensitivity to the percentile  
515 from which we start the fit (first, fifth, tenth...).

516 Fits to lognormal distributions have been carried out for the three datasets and are presented in  
517 figures 4, 6 and 5. As these fits aim at describing the tail of the PDFs, which are poorly sampled  
518 by definition, they are quite sensitive to the lack of sampling in the balloon measurements (which  
519 is accentuated by partitioning the measurements conditionally on the background wind speed).  
520 For the numerical datasets on the other hand, the fits are again found to well capture the tails of  
521 the distributions. The main point to retain from these figures is a confirmation of the relevance of  
522 the lognormal distribution for describing the tails of the PDFs, and the extension of this result to  
523 subsets of the GWMF.

## 524 **References**

525 Alexander, M., 1998: Interpretations of observed climatological patterns in stratospheric gravity  
526 wave variance. *J. Geophys. Res.*, **105 (D14)**, 8627–8640.

527 Alexander, M., 2015: Global an dseasonal variations in three-dimensional gravity wave momen-  
528 tum flux from satellite limb- sounding temperatures. *Geophys. Res. Lett.*, **42**, 6860–6867, doi:  
529 10.1002/2015GL065234.

530 Alexander, M., and Coauthors, 2008: Global estimates of gravity wave momentum flux from  
531 High Resolution Dynamics Limb Sounder Observations. *J. Geophys. Res.*, **113 (D15S18)**,  
532 doi:10.1029/2007JD008 807.

533 Alexander, M., and Coauthors, 2010: Recent developments in gravity-wave effects in climate mod-  
534 els and the global distribution of gravity-wave momentum flux from observations and models.  
535 *Q.J.R. Meteorol. Soc.*, **136**, 1103–1124.

536 Andrews, D., J. Holton, and C. Leovy, 1987: *Middle atmosphere dynamics*. Academic Press.



537 Beres, J., M. Alexander, and J. Holton, 2004: A method of specifying the gravity wave spectrum  
538 above convection based on latent heating properties and background wind. *J. Atmos. Sci.*, **61**,  
539 324–337.

540 Boccara, G., A. Hertzog, R. Vincent, and F. Vial, 2008: Estimation of gravity-wave momentum  
541 fluxes and phase speeds from long-duration stratospheric balloon flights. 1. Theory and simula-  
542 tions. *J. Atmos. Sci.*, **65**, 3042–3055.

543 Charron, M., and E. Manzini, 2002: Gravity waves from fronts: parameterization and middle  
544 atmosphere response in a general circulation model. *J. Atmos. Sci.*, **59**, 923–941.

545 de la Camara, A., and F. Lott, 2015: A parameterization of gravity waves emitted by fronts and  
546 jets. *Geophys. Res. Lett.*, **42**, 2071–2078, doi:doi:10.1002/2015GL063298.

547 de la Camara, A., F. Lott, and A. Hertzog, 2014: Intermittency in a stochastic parameterization  
548 of nonorographic gravity waves. *J. Geophys. Res. Atmos.*, **119**, 11,905–11,919, doi:10.1002/  
549 2014JD022002.

550 de la Camara, A., F. Lott, V. Jewtoukoff, R. Plougonven, and A. Hertzog, 2016: On the gravity  
551 wave forcing during the southern stratospheric final warming in LMDz. *in press for J. Atmos.*  
552 *Sci.*

553 Dunkerton, T., 1984: Inertia-gravity waves in the stratosphere. *J. Atmos. Sci.*, **41**, 3396–3404.

554 Ern, M., P. Preusse, M. Alexander, and C. Warner, 2004: Absolute values of grav-  
555 ity wave momentum flux derived from satellite data. *J. Geophys. Res.*, **109** (D20103),  
556 doi:10.1029/2006JD007327.

557 Ern, M., P. Preusse, J. Gille, C. Heppelwhite, M. Mlynczak, J. Russell III, and M. Riese,  
558 2011: Implications for atmospheric dynamics derived from global observations of gravity

559 wave momentum flux in stratosphere and mesosphere. *J. Geophys. Res.*, **116** (D19107), doi:  
560 10.1029/2011JD015821.

561 Fritts, D., and M. Alexander, 2003: Gravity wave dynamics and effects in the middle atmosphere.  
562 *Reviews of Geophysics*, **41** (1), 1003.

563 Geller, M., and J. Gong, 2010: Gravity wave kinetic, potential, and vertical fluctuation energies as  
564 indicators of different frequency gravity waves. *J. Geophys. Res.*, **115** (D11111), doi:10.1029/  
565 2009JD012266.

566 Geller, M., and Coauthors, 2013: A comparison between gravity wave momentum fluxes in obser-  
567 vations and climate models. *J. Clim.*, **26**, 6383–6405, doi:10.1175/JCLI-D-12-00545.1.

568 Hendricks, E., J. Doyle, S. Eckermann, Q. Jiang, and P. Reinecke, 2014: What is the source of the  
569 stratospheric gravity wave belt in austral winter. *J. Atmos. Sci.*, **71**, 1583–1592.

570 Hertzog, A., M. Alexander, and R. Plougonven, 2012: On the probability density functions of  
571 gravity waves momentum flux in the stratosphere. *J. Atmosph. Sci.*, **69**, 3433–3448.

572 Hertzog, A., G. Boccara, R. Vincent, F. Vial, and P. Coquerez, 2008: Estimation of gravity-wave  
573 momentum fluxes and phase speeds from long-duration stratospheric balloon flights. 2. Results  
574 from the Vorcore campaign in Antarctica. *J. Atmos. Sci.*, **65**, 3056–3070.

575 Jewtoukoff, V., A. Hertzog, R. Plougonven, A. de la Camara, and F. Lott, 2015: Gravity waves in  
576 the Southern Hemisphere derived from balloon observations and ECMWF analyses. *J. Atmos.*  
577 *Sci.*, **72**, 3449–3468.

578 Kim, Y.-J., S. Eckermann, and H.-Y. Chun, 2003: An overview of the past, present and future  
579 of gravity-wave drag parametrization for numerical climate and weather prediction models.  
580 *Atmosphere-Ocean*, **41**, 65–98.

- 581 Limpert, E., W. Stahel, and M. Abbt, 2001: Log-normal distributions across the sciences: keys  
582 and clues. *BioScience*, **51** (5), 341–352.
- 583 Lott, F., and L. Guez, 2013: A stochastic parameterization of the gravity waves due to convection  
584 and its impact on the equatorial stratosphere. *J. Geophys. Res.*, **118**, 8897–8909.
- 585 Lott, F., R. Plougonven, and J. Vanneste, 2010: Gravity waves generated by sheared potential  
586 vorticity anomalies. *J. Atmos. Sci.*, **67**, 157–170, doi:10.1175/2009JAS3134.1.
- 587 Lott, F., R. Plougonven, and J. Vanneste, 2012: Gravity waves generated by sheared three-  
588 dimensional potential vorticity anomalies. *J. Atmos. Sci.*, **69**, 2134–2151.
- 589 McLandress, C., T. Shepherd, S. Polaravapu, and S. Beagley, 2012: Is missing orographic grav-  
590 ity wave drag near 60s the cause of the stratospheric zonal wind biases in chemistry-climate  
591 models? *J. Atmos. Sci.*, **69**, 802–818.
- 592 O’Sullivan, D., and T. Dunkerton, 1995: Generation of inertia-gravity waves in a simulated life  
593 cycle of baroclinic instability. *J. Atmos. Sci.*, **52** (21), 3695–3716.
- 594 Plougonven, R., A. Hertzog, and M. Alexander, 2015: Case studies of non-orographic gravity  
595 waves over the Southern Ocean emphasize the role of moisture. *J. Geophysical Research*, **120**,  
596 doi:10.1002/2014JD022332.
- 597 Plougonven, R., A. Hertzog, and L. Guez, 2013: Gravity waves over Antarctica and the South-  
598 ern Ocean: consistent momentum fluxes in mesoscale simulations and stratospheric balloon  
599 observations. *Quart. J. Roy. Meteorolog. Soc.*, **139**, 101–118.
- 600 Plougonven, R., D. Muraki, and C. Snyder, 2005: A baroclinic instability that couples balanced  
601 motions and gravity waves. *J. Atmos. Sci.*, **62**, 1545–1559.

602 Plougonven, R., and H. Teitelbaum, 2003: Comparison of a large-scale inertia-gravity wave as  
603 seen in the ECMWF and from radiosondes. *Geophys. Res. Lett.*, **30** (18), 1954.

604 Plougonven, R., H. Teitelbaum, and V. Zeitlin, 2003: Inertia-gravity wave generation by the tro-  
605 pospheric mid-latitude jet as given by the fastex radiosoundings. *J. Geophys. Res.*, **108** (D21),  
606 4686.

607 Plougonven, R., and F. Zhang, 2014: Internal gravity waves from atmospheric jets and fronts.  
608 *Reviews of Geophysics*, **52**.

609 Rabier, F., and coauthors, 2010: The Concordiasi project in Antarctica. *Bull. American Meteor.*  
610 *Soc.*, **91** (1), 69–86.

611 Ribstein, B., U. Achatz, and F. Senf, 2015: The interaction between gravity waves and solar tides:  
612 Results from 4-d ray tracing coupled to a linear tidal model. *J. Geophys. Res. Space Phys.*, **120**,  
613 6795–6817.

614 Richter, J., F. Sassi, and R. Garcia, 2010: Toward a physically based gravity wave source pa-  
615 rameterization in a general circulation model. *J. Atmos. Sci.*, **67**, 136–156, doi:doi:10.1175/  
616 2009JAS3112.1.

617 Sato, K., S. Tateno, S. Watanabe, and Y. Kawatani, 2012: Gravity wave characteristics in the  
618 Southern Hemisphere revealed by a high-resolution middle-atmosphere general circulation  
619 model. *J. Atmos. Sci.*, **69**, 1378–1396.

620 Sato, K., S. Watanabe, Y. Kawatani, Y. Tomikawa, K. Miyazaki, and M. Takayashi,  
621 2009: On the origins of mesospheric gravity waves. *Geophys. Res. Lett.*, **36** (L19801),  
622 doi:10.1029/2009GL039908.

- 623 Sato, K., and M. Yoshiki, 2008: Gravity wave generation around the polar vortex in the strato-  
624 sphere revealed by 3-hourly radiosonde observations at Syowa Station. *J. Atmos. Sci.*, **65**, 3719–  
625 3735.
- 626 Senf, F., and U. Achatz, 2011: On the impact of middle-atmosphere thermal tides on  
627 the propagation and dissipation of gravity waves. *J. Geophys. Res.*, **116** (D24110),  
628 doi:10.1029/2011JD015794.
- 629 Shutts, G., and S. Vosper, 2011: Stratospheric gravity waves revealed in NWP forecast models.  
630 *Q.J.R. Meteorol. Soc.*, **137** (655), 303–317.
- 631 Skamarock, W., and Coauthors, 2008: A description of the Advanced Research WRF Version 3.  
632 *NCAR Technical Note*.
- 633 Song, I.-S., and H.-Y. Chun, 2005: Momentum flux spectrum of convectively forced internal  
634 gravity waves and its application to gravity wave drag parameterization. Part I: Theory. *J. Atmos.*  
635 *Sci.*, **62**, 107–124.
- 636 Vanneste, J., 2013: Balance and spontaneous wave generation in geophysical flows. *Ann. Rev.*  
637 *Fluid Mech.*, **45**, 147–172.
- 638 Vanneste, J., and I. Yavneh, 2004: Exponentially small inertia-gravity waves and the breakdown  
639 of quasi-geostrophic balance. *J. Atmos. Sci.*, **61**, 211–223.
- 640 Vanneste, J., and I. Yavneh, 2007: Unbalanced instabilities of rapidly rotating stratified shear  
641 flows. *J. Fluid Mech.*, **584**, 373–396.
- 642 Vincent, R., and A. Hertzog, 2014: The response of superpressure balloons to gravity wave mo-  
643 tions. *Atmospheric Measurement Techniques*, **7** (4), 1043–1055.

- 644 Vincent, R., A. Hertzog, G. Boccara, and F. Vial, 2007: Quasi-Lagrangian superpressure balloon  
645 measurements of gravity-wave momentum fluxes in the polar stratosphere of both hemispheres.  
646 *Geophys. Res. Lett.*, **34 (L19804)**, doi:doi:10.1029/2007GL031072.
- 647 Waite, M. L., and C. Snyder, 2012: Mesoscale energy spectra of moist baroclinic waves. *J. Atmos.*  
648 *Sci.*, **70 (4)**, 1242–1256.
- 649 Whiteway, J., T. Duck, D. Donovan, J. Bird, S. Pal, and A. Carswell, 1997: Measurements of  
650 gravity wave activity within and around the Arctic stratospheric vortex. *Geophys. Res. Lett.*,  
651 **24 (11)**, 1387–1390.
- 652 Wright, C., S. Osprey, and J. Gille, 2013: Global observations of gravity wave intermittency and  
653 its impact on the observed momentum flux morphology. *J. Geophys. Res.*, **118**, 10,98010,993,  
654 doi:10.1002/jgrd.50869.
- 655 Wu, D., and S. Eckermann, 2008: Global gravity wave variances from Aura MLS: characteristics  
656 and interpretation. *J. Atmos. Sci.*, **65 (12)**, 3695–3718.
- 657 Zhang, F., 2004: Generation of mesoscale gravity waves in upper-tropospheric jet-front systems.  
658 *J. Atmos. Sci.*, **61 (4)**, 440–457.
- 659 Zhang, F., S. Koch, C. Davis, and M. Kaplan, 2001: Wavelet analysis and the governing dynamics  
660 of a large amplitude mesoscale gravity wave event along the east coast of the united states.  
661 *Q.J.R. Meteorol. Soc.*, **127**, 2209–2245.
- 662 Zülicke, C., and D. Peters, 2006: Simulation of inertia-gravity waves in a poleward breaking  
663 Rossby wave. *J. Atmos. Sci.*, **63**, 3253–3276.
- 664 Zülicke, C., and D. Peters, 2008: Parameterization of strong stratospheric inertigravity waves  
665 forced by poleward-breaking rossby waves. *Mon. Wea. Rev.*, **136**, 98–119.

666 **LIST OF TABLES**

667 **Table 1.** Summary of the resolution and expected limitations of the three datasets used  
668 to diagnose the relation between gravity waves and background wind speed.  
669 The last column provides an estimate of the horizontal wavelength ( $\lambda_h$ ) and  
670 vertical wavelength ( $\lambda_v$ ) that can confidently be resolved. . . . . 32

Dataset	Resolution	Observed waves
WRF simulations	$dx = 20$ km, $dz$ 300 m	$\lambda_h > 120$ km, $\lambda_z > 2$ km
ECMWF analyses	$dx$ 13 km, $dz$ 500 m	$\lambda_h > 80$ km, $\lambda_z > 3$ km
Concordiasi balloons	Measurements every minute	Whole spectrum: $f < \hat{\omega} < N$ .

671 TABLE 1. Summary of the resolution and expected limitations of the three datasets used to diagnose the rela-  
672 tion between gravity waves and background wind speed. The last column provides an estimate of the horizontal  
673 wavelength ( $\lambda_h$ ) and vertical wavelength ( $\lambda_z$ ) that can confidently be resolved.



674 **LIST OF FIGURES**

675 **Fig. 1.** Two examples of snapshots of absolute momentum fluxes (colors, logarithmic scale) and  
676 wind speed (thick gray lines for isotachs 20 and 40  $\text{m s}^{-1}$ , thick black line for 60  $\text{m s}^{-1}$ ) at  
677 an altitude of  $z = 20$  km, from the mesoscale simulations of the flow above Antarctica and  
678 the Southern Ocean (Plougonven et al. 2013). The dates are October 23rd, 18:00UTC for  
679 the top panel, November 7th, 2005, 12:00UTC for the bottom panel. . . . . 35

680 **Fig. 2.** Mean winds in the ECMWF. . . . . 36

681 **Fig. 3.** Mean winds in WRF. . . . . 37

682 **Fig. 4.** Probability Density Functions of the gravity wave momentum fluxes (GWMF) in mPa from  
683 the WRF simulations, at  $z = 20$  km, conditional on the background wind. . . . . 38

684 **Fig. 5.** Same as Figure 4 but for the momentum fluxes calculated from the ECMWF analyses, for  
685 the time of the Concordiasi campaign, September 2010 to January 2011. . . . . 39

686 **Fig. 6.** Same as Figure 4 but for the long-duration balloons of the Concordiasi campaign, September  
687 2010 to January 2011. . . . . 40

688 **Fig. 7.** Normalized medians of the PDFs of GWMF (upper plots) and geometric standard deviations  
689 (lower plots) as a function of the background wind speed. The left column shows these  
690 quantities directly obtained from the values of GWMF, whereas the right column shows  
691 these quantities obtained for the lognormal fits. Black symbols correspond to the mesoscale  
692 simulations, red symbols to the ECMWF output, and blue symbols to the Concordiasi bal-  
693 loons. The medians were normalized by the means of the medians found for winds between  
694 20 and 40  $\text{m s}^{-1}$ . For the medians, the linear regressions (thin lines) are also displayed. . . . . 41

695 **Fig. 8.** PDFs of momentum fluxes conditional on the background wind speed at four different  
696 heights in the WRF simulations:  $z = 12$  km (upper-left),  $z = 16$  km (upper-right),  $z = 25$  km  
697 (lower-left) and  $z = 30$  km (lower-right). . . . . 42

698 **Fig. 9.** Variation of the normalized median of GWMF with background wind speed  $U$ , from the  
699 WRF simulations (left) and the ECMWF analyses (right) for different heights (see legend in  
700 each graph). . . . . 43

701 **Fig. 10.** PDFs of gravity wave momentum fluxes at 30 km, in the WRF simulations, conditional on  
702 the wind speed at 10 km. . . . . 44

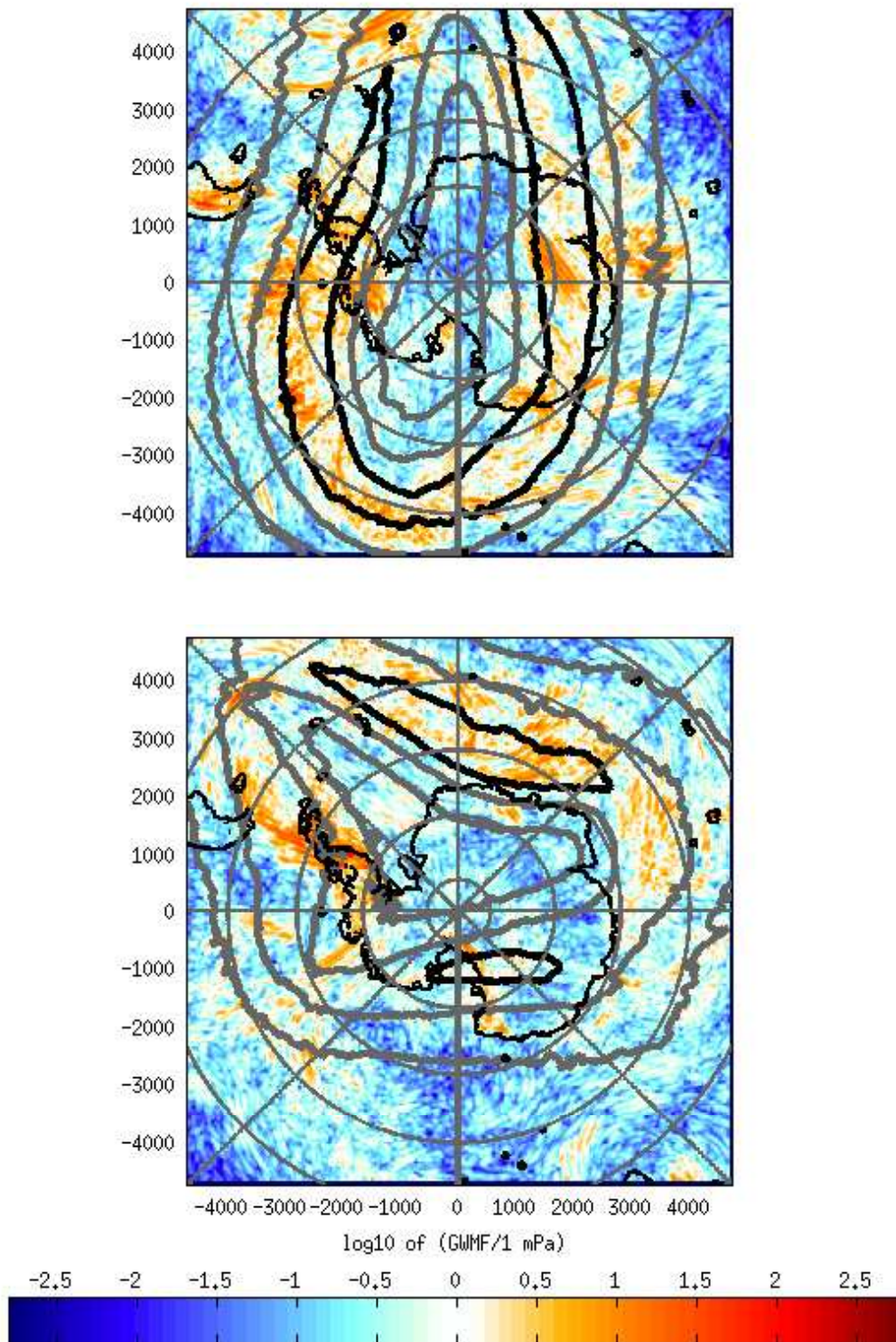
703 **Fig. 11.** PDF of the orientation of momentum fluxes relative to the local flow, at  $z = 20$  km and over  
704 the ocean, from the WRF simulations. . . . . 45

705 **Fig. 12.** PDFs of GWMF at  $z = 10$  km conditional on different indicators of tropospheric jet/front  
706 activity. First panel: conditional on the absolute value of surface vorticity, by increments  
707 of  $0.5 \cdot 10^{-4} \text{ s}^{-1}$ . Second panel: conditional on the absolute value of relative vorticity at  $z =$   
708  $5$  km, by increments of  $0.5 \cdot 10^{-4} \text{ s}^{-1}$ . Third panel: conditional on surface pressure anomaly,  
709 sorted by increments of 10 hPa. . . . . 46

710 **Fig. 13.** PDFs of GWMF conditional on the absolute values of relative vorticity at the surface (top)  
711 and at the mid-troposphere (bottom), averaged in boxes that are 10 degrees longitude by 5  
712 degrees latitude. . . . . 47

713 **Fig. 14.** Same as Figure 4 but for the GWMF from the offline parameterization, for the period from  
714 September 2010 to January 2011. The left column shows results for the parameterization  
715 used with the source varying with the tropospheric flow (see de la Camara and Lott (2015)  
716 for details). The right column shows results using a source which retains a lognormal distri-  
717 bution but with the amplitudes independent of the tropospheric flow. The standard deviations  
718 for the phase speeds are  $40 \text{ m s}^{-1}$  for the upper panels, and  $10 \text{ m s}^{-1}$  for the lower panels. . . . 48

719 **Fig. 15.** Example of the fit using a lognormal, for the PDF of momentum fluxes found over the ocean  
720 at  $z = 20 \text{ km}$  in the WRF simulations, for background winds larger than  $50 \text{ m s}^{-1}$ . Three lines  
721 are shown: the thick black line is for the PDF estimated using 200 bins equally spaced for  
722 the logarithm of momentum fluxes, the thin black line depicts the lognormal PDF with the  
723 same median and geometric standard deviation, the red line is the optimized lognormal PDF.  
724 Top panel: standard plot of the PDF, showing the emphasis of values near zero (horizontal  
725 axis only extends to 6 mPa). Bottom panel: semilog view of the complete distribution. . . . 49



726 FIG. 1. Two examples of snapshots of absolute momentum fluxes (colors, logarithmic scale) and wind speed  
 727 (thick gray lines for isotachs 20 and 40  $\text{ms}^{-1}$ , thick black line for 60  $\text{ms}^{-1}$ ) at an altitude of  $z = 20$  km, from  
 728 the mesoscale simulations of the flow above Antarctica and the Southern Ocean (Plougonven et al. 2013). The  
 729 dates are October 23rd, 18:00UTC for the top panel, November 7th, 2005, 12:00UTC for the bottom panel.

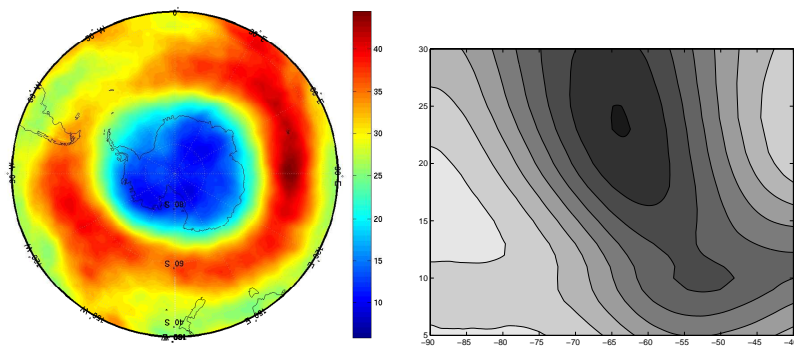


FIG. 2. Mean winds in the ECMWF.

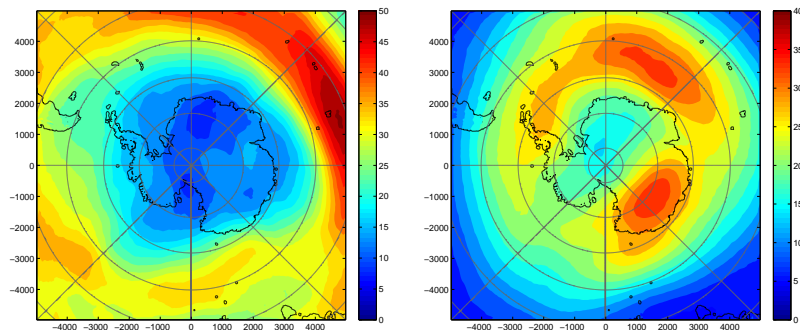
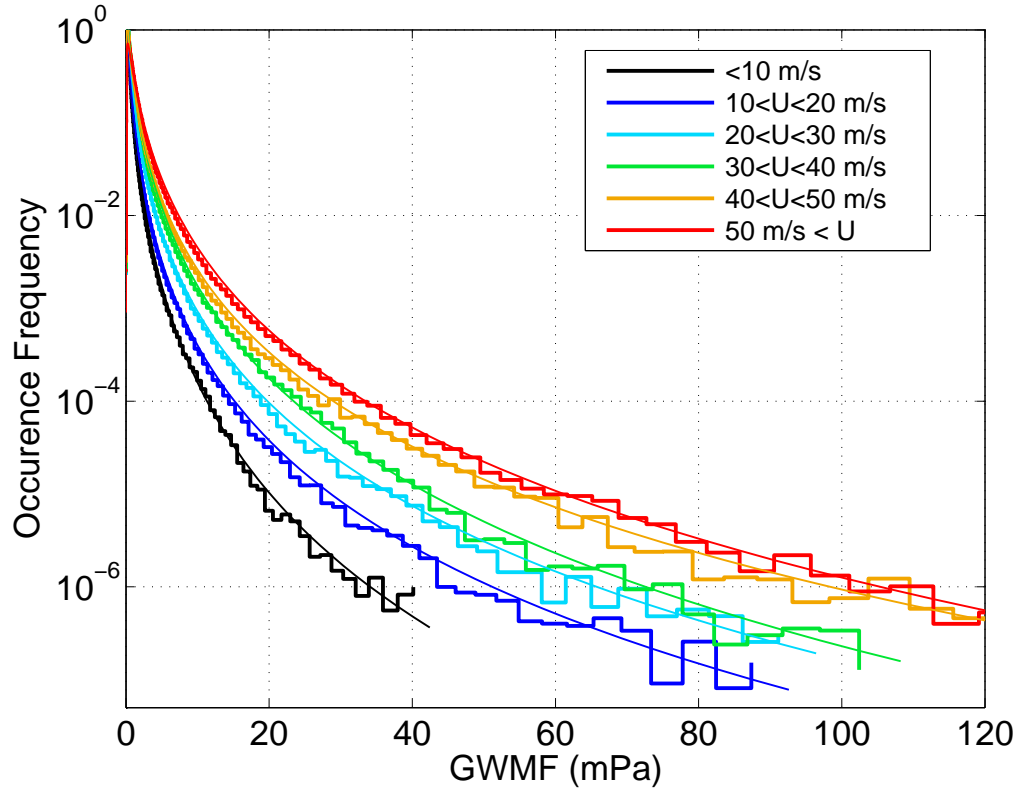
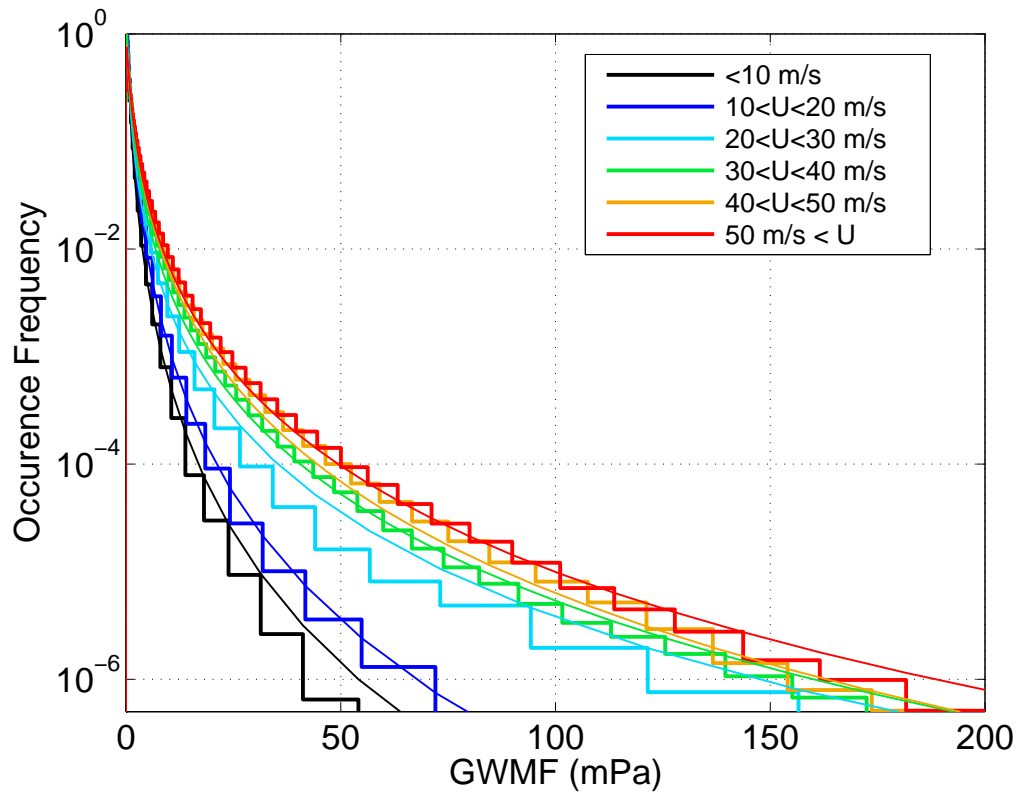


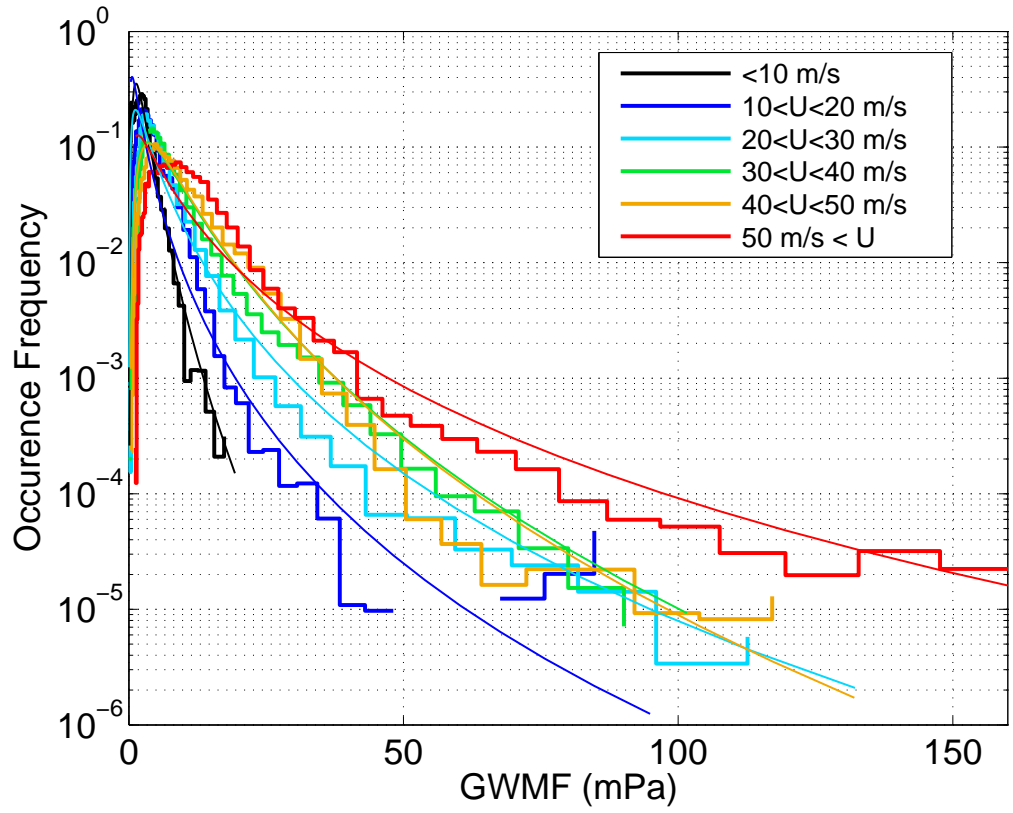
FIG. 3. Mean winds in WRF.



730 FIG. 4. Probability Density Functions of the gravity wave momentum fluxes (GWMF) in mPa from the WRF  
 731 simulations, at  $z = 20$  km, conditional on the background wind.

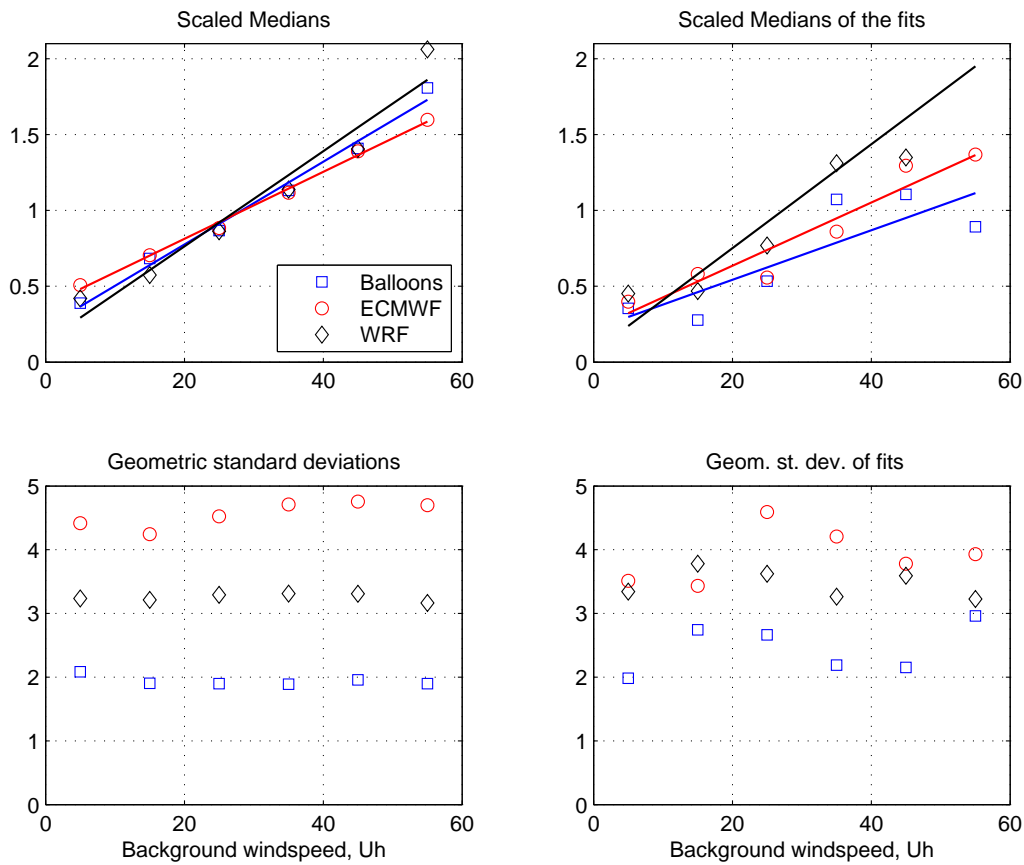


732 FIG. 5. Same as Figure 4 but for the momentum fluxes calculated from the ECMWF analyses, for the time of  
 733 the Concordiasi campaign, September 2010 to January 2011.

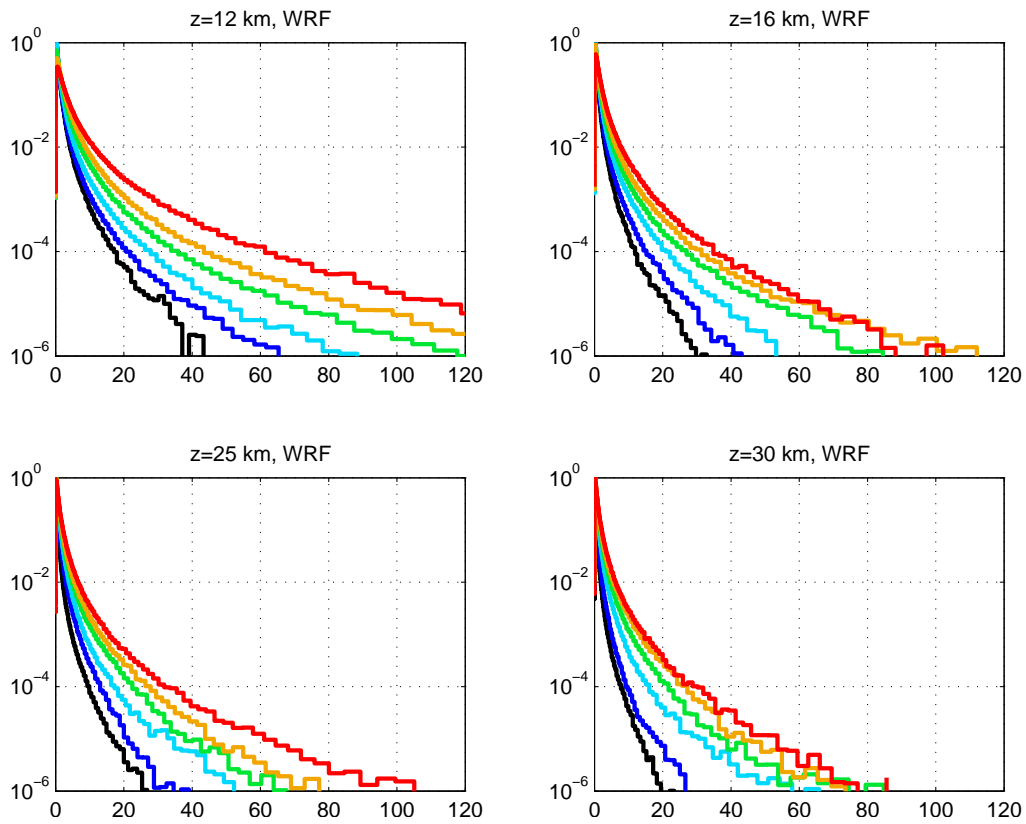


734 FIG. 6. Same as Figure 4 but for the long-duration balloons of the Concordiasi campaign, September 2010 to  
 735 January 2011.

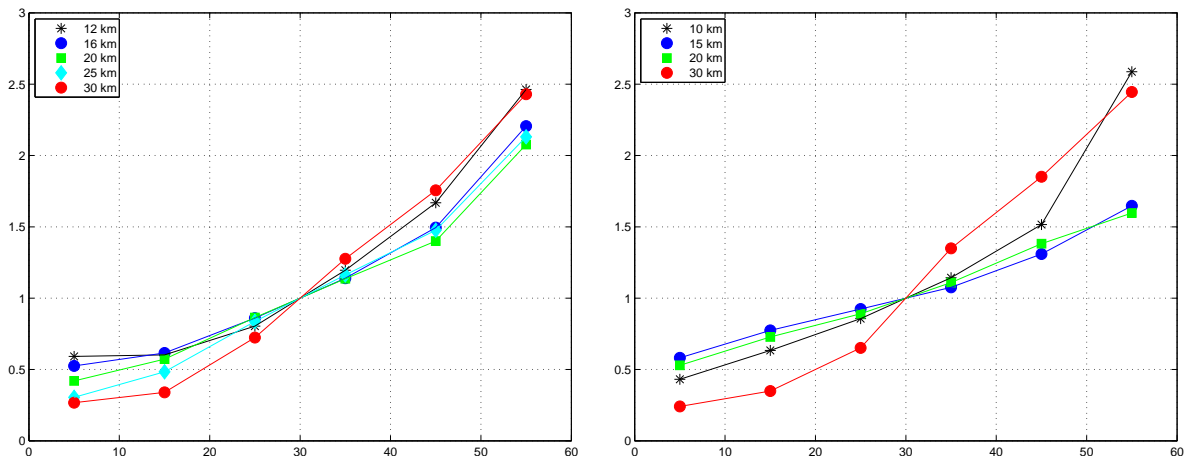




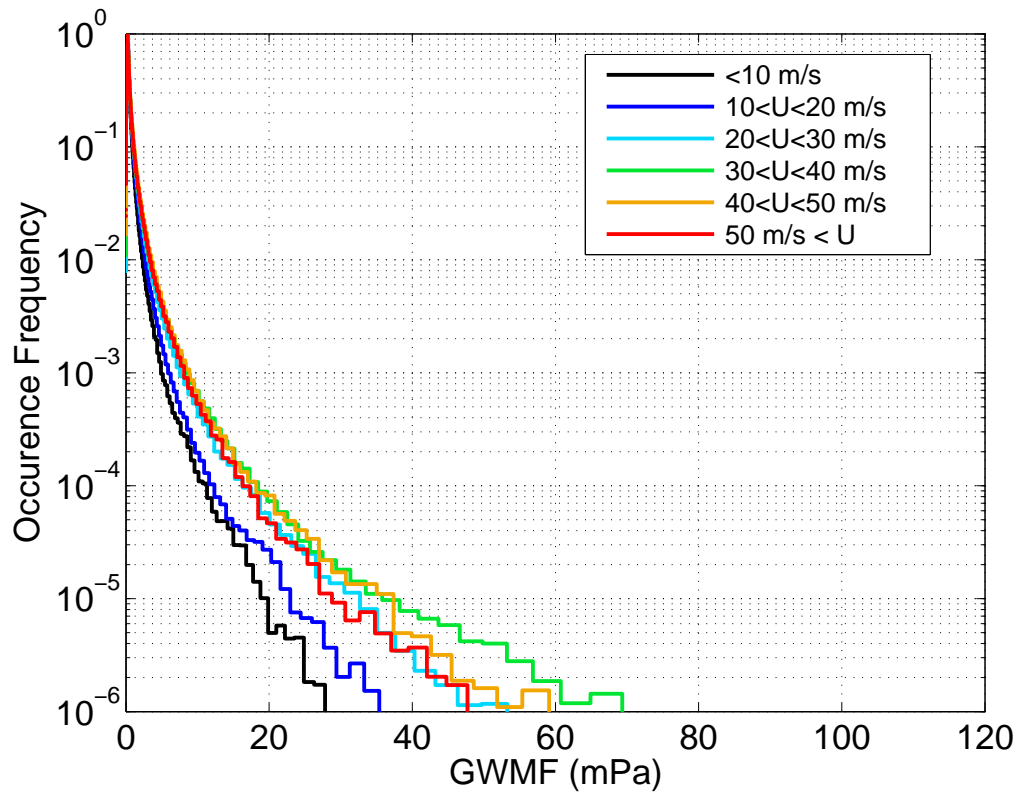
736 FIG. 7. Normalized medians of the PDFs of GWMF (upper plots) and geometric standard deviations (lower  
 737 plots) as a function of the background wind speed. The left column shows these quantities directly obtained from  
 738 the values of GWMF, whereas the right column shows these quantities obtained for the lognormal fits. Black  
 739 symbols correspond to the mesoscale simulations, red symbols to the ECMWF output, and blue symbols to the  
 740 Concordiasi balloons. The medians were normalized by the means of the medians found for winds between 20  
 741 and  $40 \text{ m s}^{-1}$ . For the medians, the linear regressions (thin lines) are also displayed.



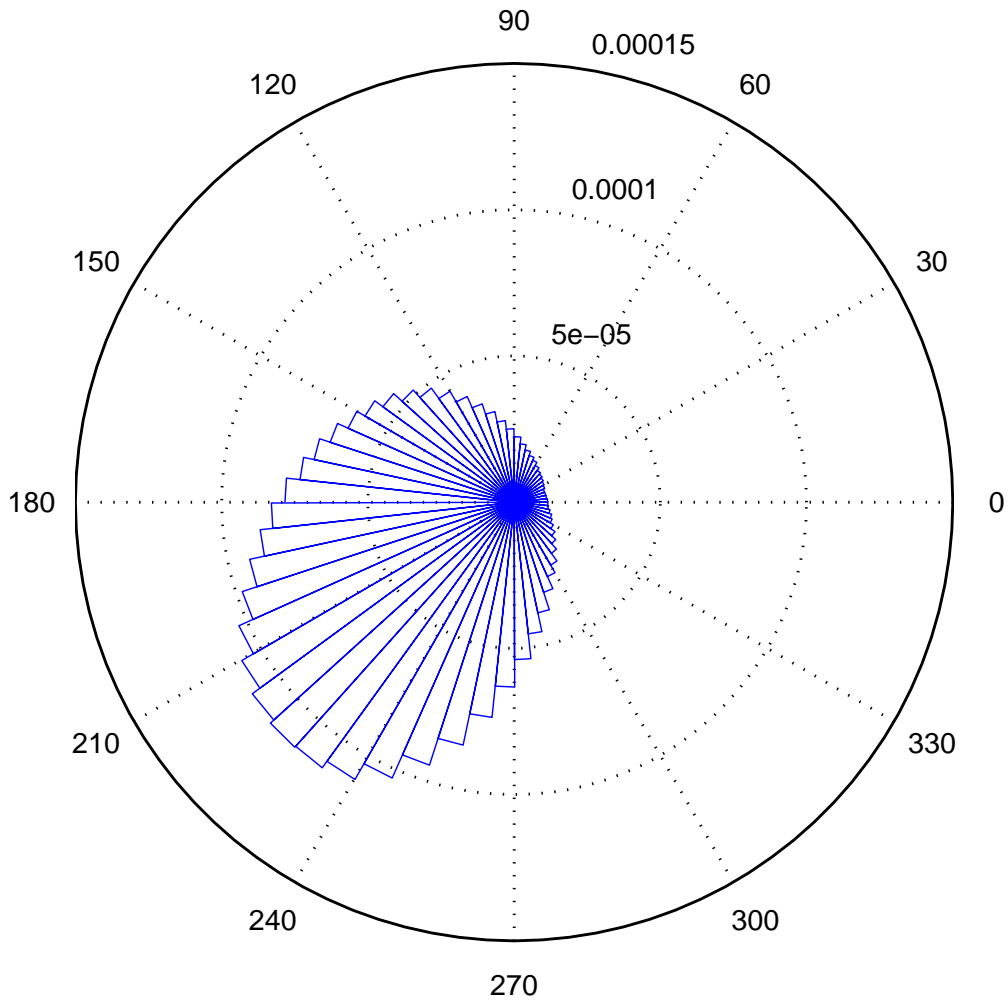
742 FIG. 8. PDFs of momentum fluxes conditional on the background wind speed at four different heights in  
 743 the WRF simulations:  $z = 12$  km (upper-left),  $z = 16$  km (upper-right),  $z = 25$  km (lower-left) and  $z = 30$  km  
 744 (lower-right). .



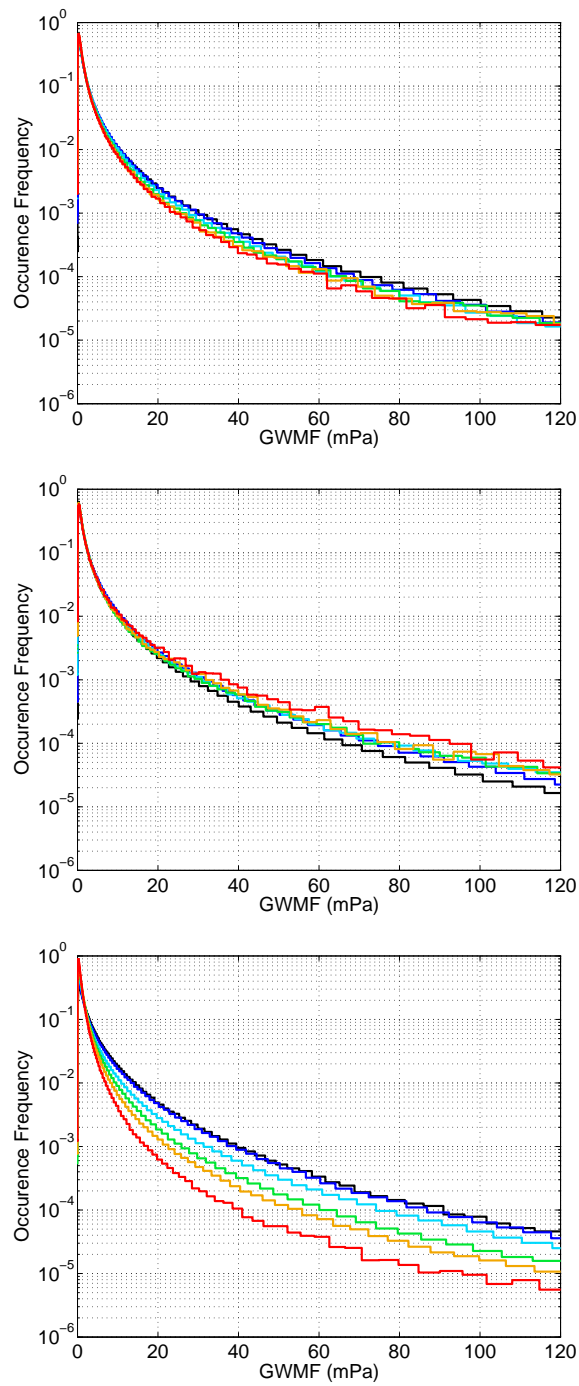
745 FIG. 9. Variation of the **normalized** median of GWMF with background wind speed  $U$ , from the WRF  
 746 simulations (left) and the ECMWF analyses (right) for different heights (see legend in each graph).



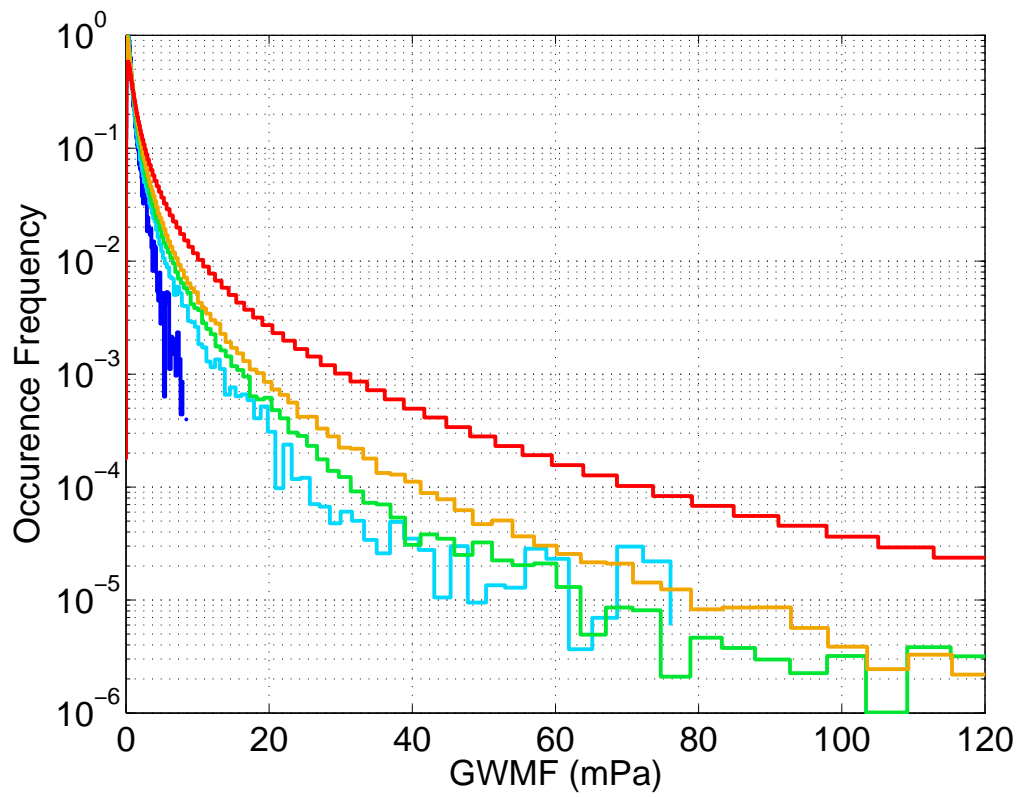
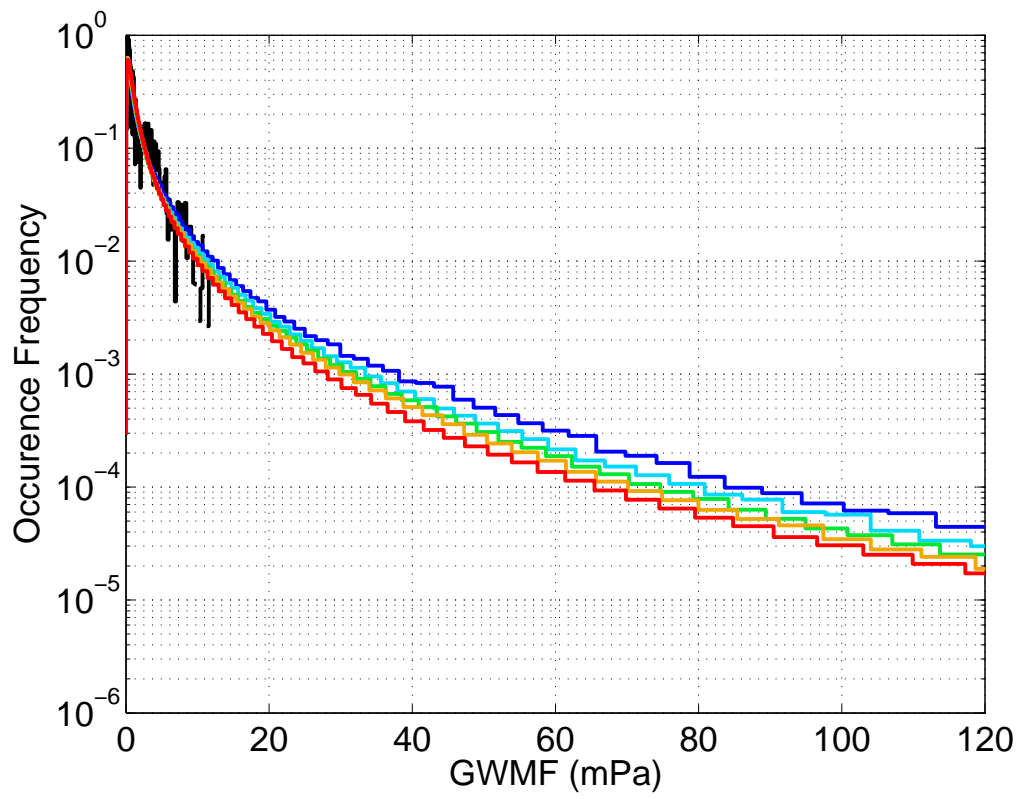
747 FIG. 10. PDFs of gravity wave momentum fluxes at 30 km, in the WRF simulations, conditional on the wind  
 748 speed at 10 km.



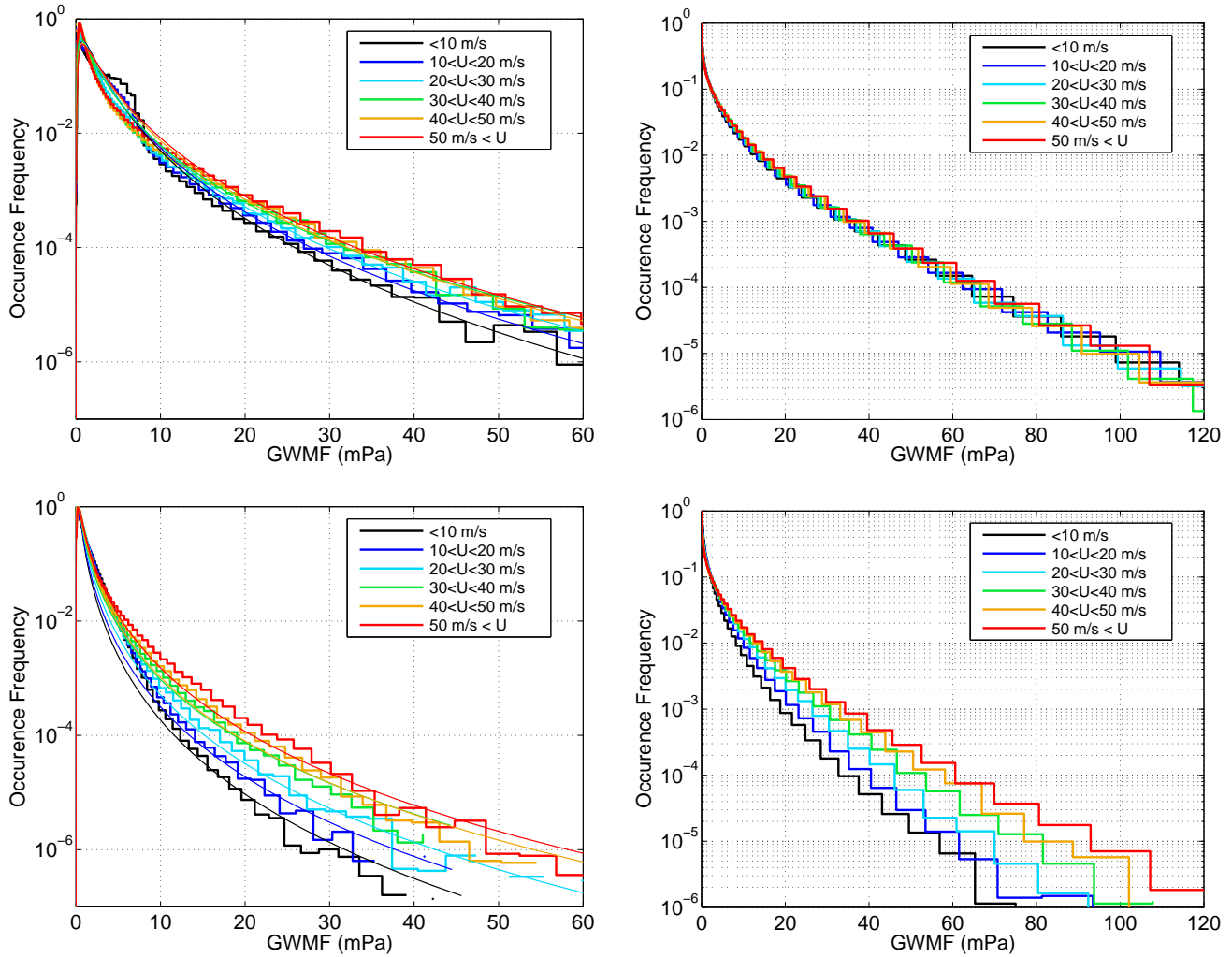
749 FIG. 11. PDF of the orientation of momentum fluxes relative to the local flow, at  $z = 20$  km and over the  
 750 ocean, from the WRF simulations.



751 FIG. 12. PDFs of GWMF at  $z = 10\text{km}$  conditional on different indicators of tropospheric jet/front activity.  
 752 First panel: conditional on the absolute value of surface vorticity, by increments of  $0.5 \cdot 10^{-4} \text{ s}^{-1}$ . Second panel:  
 753 conditional on the absolute value of relative vorticity at  $z = 5\text{km}$ , by increments of  $0.5 \cdot 10^{-4} \text{ s}^{-1}$ . Third panel:  
 754 conditional on surface pressure anomaly, sorted by increments of 10 hPa.

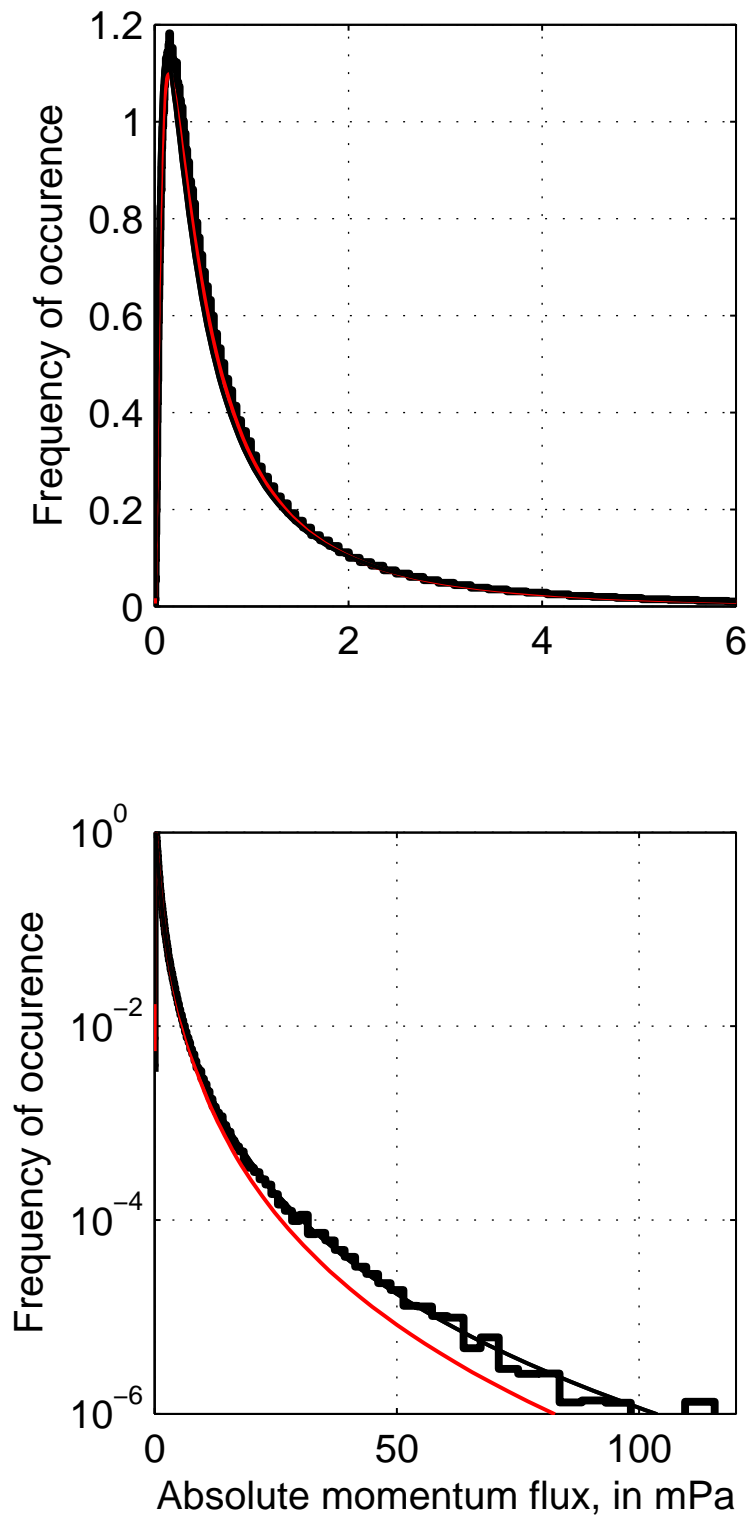


755 FIG. 13. PDFs of GWMF conditional on the absolute values of relative vorticity at the surface (top) and at the  
 756 mid-troposphere (bottom), averaged in boxes that are 10 degrees longitude by 5 degrees latitude.



757 FIG. 14. Same as Figure 4 but for the GWMF from the offline parameterization, for the period from September  
 758 2010 to January 2011. The left column shows results for the parameterization used with the source varying with  
 759 the tropospheric flow (see de la Camara and Lott (2015) for details). The right column shows results using a  
 760 source which retains a lognormal distribution but with the amplitudes independent of the tropospheric flow. The  
 761 standard deviations for the phase speeds are  $40 \text{ m s}^{-1}$  for the upper panels, and  $10 \text{ m s}^{-1}$  for the lower panels.





762 FIG. 15. Example of the fit using a lognormal, for the PDF of momentum fluxes found over the ocean at  
 763  $z = 20\text{km}$  in the WRF simulations, for background winds larger than  $50\text{ m s}^{-1}$ . Three lines are shown: the thick  
 764 black line is for the PDF estimated using 200 bins equally spaced for the logarithm of momentum fluxes, the  
 765 thin black line depicts the lognormal PDF with the same median and geometric standard deviation, the red line  
 766 is the optimized lognormal PDF. Top panel: standard plot of the PDF, showing the emphasis of values near zero  
 767 (horizontal axis only extends to 6 mPa). Bottom panel: semilog view of the complete distribution.